

Authors are encouraged to submit new papers to INFORMS journals by means of a style file template, which includes the journal title. However, use of a template does not certify that the paper has been accepted for publication in the named journal. INFORMS journal templates are for the exclusive purpose of submitting to an INFORMS journal and should not be used to distribute the papers in print or online or to submit the papers to another publication.

Two-stage Models for Flood Mitigation of Electrical Substations

Brent Austgen, Erhan Kutanoglu, John J. Hasenbein

The University of Texas at Austin, Operations Research and Industrial Engineering Program

Surya Santoso

The University of Texas at Austin, Chandra Department of Electrical and Computer Engineering

We compare stochastic programming and robust optimization decision models for informing the deployment of temporary flood mitigation measures to protect electrical substations prior to an imminent and uncertain hurricane. In our models, the first stage captures the deployment of a fixed quantity of flood mitigation resources, and the second stage captures the operation of a potentially degraded power grid with the primary goal of minimizing load shed. To model grid operation, we introduce novel adaptations of the DC and LPAC power flow approximation models that feature relatively complete recourse by way of a blackout indicator variable and relaxed model of power generation. We apply our models to a pair of geographically realistic flooding case studies, one based on Hurricane Harvey and the other on Tropical Storm Imelda. We investigate the effect of the mitigation budget, the choice of power flow model, and the uncertainty perspective on the optimal mitigation strategy. Our results indicate the mitigation budget and uncertainty perspective are impactful whereas the choice of power flow model is of little to no consequence.

Key words: stochastic programming; robust optimization; power flow; flooding; hurricane; resilience; mitigation; risk management

1. Introduction

The power grid underpins or is codependent with many lifeline infrastructure systems including water, natural gas, transportation, and communication. Power grid resilience is obviously crucial to humankind's well-being; however, it is also vulnerable especially to extreme weather. According to information collected by the United States Department of Energy via form DOE-417, the number of widespread outages caused by severe weather and natural disasters has increased from around 40 annually in the early 2000's to about 80 by 2010 to

100 or more in recent years (ISER2023). Many of the worst outages and economic losses are due to tropical cyclones (NCEI2022), and many climate models project the frequency and intensity of the most extreme tropical cyclones (*i.e.*, Category 4 and Category 5 storms) to increase globally (Webster et al. 2005, Knutson et al. 2020), thus motivating the continued study and pursuit of power grid resilience.

In decision models, power grid physics and operation are captured by a power flow (PF) model. The exact model for AC power flow (ACPF) is nonconvex and thus computationally difficult in many decision making applications. However, a variety of tractable surrogate models may be formed by approximating, relaxing, or restricting the exact model (Molzahn and Hiskens 2019). In deciding which PF model to use for an application, the trade-off between a model’s fidelity and computational ease is a major consideration.

In our application, we consider the mitigation of flood-induced component outages via deployment of temporary flood barriers like Tiger DamsTM in the hours leading up to an imminent hurricane’s landfall. The discrete mitigation decisions and flooding uncertainty induce combinatorial effects on the grid topology which require the conditional enforcement of certain physical laws (*e.g.*, only enforce Ohm’s Law on closed circuits). Due to these inherent complexities and the time-sensitive nature of the decision making in our application, we only consider incorporating simple linear and convex quadratic PF approximations. Even among these simple PF models, there is considerable variation in fidelity and complexity.

In this paper, we submit a computational study designed to determine which PF model is most appropriate for our flood mitigation application. Throughout, we deliver the following contributions:

1. We incorporate a novel blackout indicator variable, bus and branch indicator variables, and a flexible model of generation into two widely used surrogate PF models, namely the ubiquitous DC approximation and the more contemporary linear programming AC (LPAC) approximation (Coffrin and Van Hentenryck 2014). These adaptations, and particularly the blackout indicator variable, guarantee that the PF models always have a feasible “blackout” solution in which no power is generated and no loads are satisfied. To the best of our knowledge, we are the first to take such an approach to severe contingency planning.
2. We embed our adapted PF models in two-stage stochastic programming and robust optimization models that capture the preemptive deployment of flood mitigation and

the consequences of unmitigated substation flooding on the power grid. Because the PF models are feasible, the two-stage models feature relatively complete recourse, and this allows the models to prescribe mitigation solutions even one or more contingencies are capable of inducing a grid-wide blackout.

3. Applying the two-stage models to two geographically realistic case studies hurricane-induced flooding in the Texas coastal region, we assess the impact of the chosen surrogate PF model, the uncertainty perspective, and the mitigation budget on the optimal flood mitigation. Our results suggest the chosen surrogate PF model has almost no impact whereas the uncertainty perspective and resource budget have a major effect. Because the LPAC approximation is more complex computationally, we deduce the DC approximation is preferred for this resilience application.
4. Our models, methodology, and analysis may serve as a guide for determining which PF models are best in different applications, especially those in which the important decisions are affected by but do not directly pertain to power flow.

The remainder of the paper is structured as follows. Section 2 provides a review of literature pertaining to resilience, PF modeling, and comparisons of PF models. In Section 3, we introduce our novel adaptations of the DC and LPAC power flow approximation models and their incorporation in overarching two-stage stochastic programming and robust optimization models designed to inform flood mitigation decisions for electric substations. In Section 4, we compare the models using results obtained from applying the models to the flooding case studies. Finally, we present our conclusions in Section 5.

2. Literature Review

2.1. Reliability, Resilience, and Risk

Power grid contingency planning has historically revolved around optimizing reliability objectives and satisfying reliability criteria. For a variety of reasons, such objectives and criteria are inappropriate or inadequate for planning against high-impact, low-frequency (HILF) threats such as hurricanes. Many reliability metrics like System Average Interruption Frequency Index (SAIFI), System Average Interruption Duration Index (SAIDI), and others from the IEEE Guide for Electric Power Distribution Reliability Indices standards document (IEEE2022) are typically computed from historical data to evaluate performance. Using these look-behind metrics to evaluate anticipated performance is difficult because it requires

incorporating an intractable level of temporal detail into the models. These indices are generally applied to residential customers affected by reliability events originating within the distribution system, but the consequences of hurricanes are seldom confined to distribution systems.

Researchers have studied security-constrained optimal power flow (SCOPF) for at least 35 years (Monticelli et al. 1987) to evaluate system performance during predetermined contingencies. In SCOPF, the contingencies are often based on the $N - 1$ reliability criterion (Zhang et al. 2012, Dvorkin et al. 2018) that the North American Electric Reliability Corporation maintains as a reliability standard (NERC2022) or the more general $N - k$ reliability criterion (Huang et al. 2022). As highlighted in Moreno et al. (2020), reliability criteria are useful for building infrastructure capable of reacting to contingencies but not so much for building infrastructure capable of withstanding threats such that contingencies do not even arise. Additionally, hurricanes often engender consequences too severe for “secure” grid operation to be possible, and imminent hurricanes are typically forecast with some accuracy. That said, the SCOPF model is too rigid, the $N - 1$ contingencies too mild, and the $N - k$ contingencies too broad for our application.

We instead adopt an approach based on risk and resilience. There are a variety of definitions for these terms in the literature. One of the most popular definitions of resilience comes from a 2012 report by the National Research Council (NRC2012): “Resilience is the ability to prepare and plan for, absorb, recover from, and more successfully adapt to adverse events.” More nuanced aspects of risk and resilience are debated. For example, risk and resilience as defined in Linkov and Trump (2019) are respectively threat-dependent and threat-agnostic. However, in Logan et al. (2022), resilience is defined as being system- and context-specific and inherently integrated with risk such that the two are only reasonably assessed together. We adopt the latter perspective in our work and develop our model according to the conceptual framework in Watson et al. (2014) that proposes resilience metrics be formed with consideration of three key factors: the threat, the likelihood, and the consequences. We incorporate a notion of risk through a risk measure. Namely, we employ as risk measures the expectation operator associated with stochastic programming (SP) (Birge and Louveaux 2011) and the maximum operator associated with robust optimization (RO) (Ben-Tal et al. 2009). We capture the threat and likelihoods by considering a sample distribution of representative hurricane flooding scenarios. Consequences in each scenario are a function of the

flooding realization and preparedness decisions, and they are determined by an OPF model that captures the post-disaster, pre-recovery system state.

2.2. Power Flow Modeling

There are many examples of surrogate PF models being incorporated into optimization models for power grid resilience to natural disasters. Examples include the network flow relaxation for general distribution system hardening (Tan et al. 2018) and grid operation during a progressing wildfire (Mohagheghi and Rebennack 2015); the DC power transfer distribution factor (PTDF) approximation for winter storm mitigation planning (Garcia et al. 2022); the DC B-theta approximation for hurricane restoration planning (Arab et al. 2015), hurricane mitigation planning (Shukla et al. 2021, 2022, Movahednia and Kargarian 2022), winter storm mitigation planning (Pierre et al. 2018), inventory stockpiling (Coffrin et al. 2011), and proactive grid posturing (Sahraei-Ardakani and Ou 2017, Quarm et al. 2022); the LPAC approximation for transmission system restoration (Coffrin and Van Hentenryck 2015); and the second-order cone programming (SOCP) relaxation for transmission system hardening (Garifi et al. 2022).

In the aforementioned research, most grid instances to which optimization models were applied comprised around 100 buses. The largest grid instances studied were the ACTIVS 2000-bus synthetic grid of Texas (Birchfield et al. 2017) and a 1263-bus grid representative of Puerto Rico (Elizondo et al. 2020) used by Garcia et al. (2022) and Quarm et al. (2022), respectively. The models in these papers incorporate linear DC approximations of PF but have a static grid topology in each contingency scenario. In this paper, we appropriate an adaptation of the DC approximation that allows the grid topology to vary as a function of both the contingency and the resilience decisions as in Pierre et al. (2018), Movahednia and Kargarian (2022), and Garifi et al. (2022) and furthermore allows total blackouts to occur for the sake of model feasibility. We apply our PF model to the coast-focused reduced network of the ACTIVS 2000-bus grid comprising 663 buses (Austgen et al. 2021, 2022, Souto et al. 2022).

2.3. Power Flow Model Comparisons

The AC power flow model is nonconvex, so embedding it in stochastic mixed-integer optimization models like ours generally yields an intractable problem. Choosing a surrogate PF model from the many that exist is difficult because there exists a trade-off between fidelity

and complexity. Incorporating a more fidelitous PF model might sacrifice computational tractability while incorporating a less fidelitous PF model might compromise the overarching optimization model’s ability to prescribe good decisions. A good example of the latter issue is that solutions to DC OPF are never feasible in the exact model under some mild assumptions (Baker 2021).

This trade-off has been studied for a variety of power systems applications. Some example comparisons are the DC and exact AC models in the context of system reliability (Kile et al. 2014), the DC and SOCP models in the context of transmission system hardening (Garifi et al. 2022), and the DC and LPAC models in the contexts of system operation (Coffrin and Van Hentenryck 2014) and system restoration (Coffrin and Van Hentenryck 2015). In each of these studies, the authors concluded the solutions of the DC model are typically worse than those of the higher-fidelity alternative in the context of an AC model feasibility study. The studies on system hardening and system restoration also concluded that decisions not directly in the scope of PF, like mitigation investments and restoration scheduling, sometimes differed substantially depending on the incorporated PF model. In contrast, Overbye et al. (2004) concluded that the DC model yields locational marginal price (LMP) values comparable to those yielded by the AC model. We perform a similar comparison of the DC and LPAC models in this paper with a focus on their impact on the optimal flood mitigation decisions. Importantly, we solve every instance to certified optimality to ensure fairer solution comparisons and avoid the potential issue of the existence of multiple qualitatively diverse near-optimal mitigation strategies.

3. Modeling

For the sake of modeling, the power grid may be viewed as a graph with buses as nodes and branches (*i.e.*, transmission lines and transformers) as edges. When a substation floods, we model all its buses and transformers, incident transmission lines, and associated generators as inoperable, and all its associated loads as unsatisfiable. This is illustrated in Figure 1. We suppose at each substation that a discrete set of resilience levels are available for implementation by stacking temporary flood barriers like Tiger DamsTM, and we use a PF model to assess the load shed that results in each scenario.

3.1. Notation

We now introduce the sets, parameters, and decision variables used in our models.

Sets

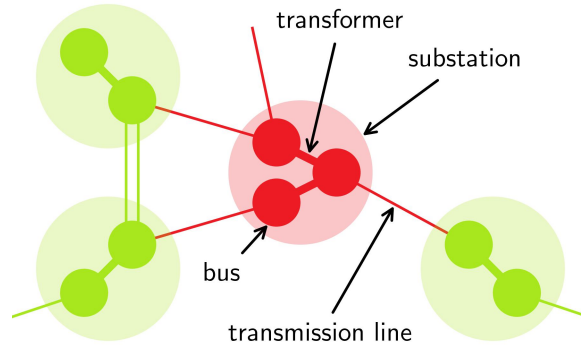


Figure 1 When a substation floods, its contained buses and transformers and all incident transmission lines become inoperable.

K	set of substations
$R = \{0, 1, \dots, \hat{r}\}$	set of resilience levels
Ω	set of scenarios
N, N_k	set of buses, buses at substation k
E	set of edges (in LPAC, $E = E^T \cup E^F$, the union of ‘to’ and ‘from’ edges)
G, G_n	set of generators, generators at bus n
D, D_n	set of loads, loads at bus n
L, L_{nm}	set of branches, branches defined on edge (n, m)
L_n^-, L_n^+, L_n	set of branches away from node n , toward node n , incident to node n
$\Theta_{\cos} \subseteq [-\pi, \pi]$	set of tangent line intersection points in the polyhedral relaxation of cosine
$\Theta_{\text{disc}} \subseteq [0, 2\pi]$	set of tangent line intersection points in the polyhedral relaxation of a disc

Parameters

$\Pr(\omega)$	probability of scenario ω occurring
$\lambda^{\text{shed}}, \lambda^{\text{over}}$	unitless objective weights for load shed and overgeneration
c_{kr}	marginal resource cost of reinforcing substation k to resilience level r from level $r - 1$
f	resource budget
ξ_{kr}	flooding uncertainty; 1 if substation k is flooded to level r ; 0 otherwise
b_l, g_l	susceptance and conductance of branch l

$\underline{p}_g^{\text{gen}}, \underline{q}_g^{\text{gen}}$	lower bounds for active and reactive power generation at generator g
$\overline{p}_g^{\text{gen}}, \overline{q}_g^{\text{gen}}$	upper bounds for active and reactive power generation at generator g
$p_d^{\text{load}}, q_d^{\text{load}}$	active and reactive power demand of load d
$\overline{s}_l^{\text{flow}}$	upper bound of apparent power flow across branch l
$\underline{v}_n, v_n, \overline{v}_n$	minimum, target, and maximum voltage magnitudes of bus n
n_{ref}	reference bus
$\overline{\theta}_{\Delta}$	maximum voltage phase angle difference of adjacent buses
$\overline{\theta}$	maximum absolute voltage phase angle for any bus in the system
M	arbitrarily large positive constant (for big- M method)

Decision Variables

$x_{kr} \in \{0, 1\}$	flood mitigation indicator variable; 1 if substation k is resilient to level r , 0 otherwise
$\chi \in \{0, 1\}$	blackout indicator variable; 1 if a blackout occurs, 0 otherwise
$\alpha_n \in \{0, 1\}$	bus status indicator variable; 1 if bus n is operational, 0 otherwise
$\beta_{nm} \in \{0, 1\}$	branch status indicator variable; 1 if branches on edge (n, m) are operational, 0 otherwise
$\hat{p}_g \in \mathbb{R}, \hat{q}_g \in \mathbb{R}$	active and reactive power generation at generator g
$\check{p}_g \in \mathbb{R}_+$	active power overgeneration at generator g
$\tilde{p}_l \in \mathbb{R}, \tilde{q}_l \in \mathbb{R}$	active and reactive power flow across branch l
$\delta_d \in [0, 1]$	proportion of load d satisfied
$\theta_n \in [-\overline{\theta}, \overline{\theta}]$	voltage phase angle of bus n
$\widehat{\sin}_{nm} \in \mathbb{R}$	approximation of $\sin(\theta_n - \theta_m)$
$\widehat{\cos}_{nm} \in [\cos(\overline{\theta}_{\Delta}), 1]$	approximation of $\cos(\theta_n - \theta_m)$
$\phi_n \in \mathbb{R}$	deviation from target voltage magnitude at bus n

We aim to denote similar types of parameters and variables similarly. For example, all power flow variables have a tilde (*e.g.*, \tilde{p}_l and \tilde{q}_l), and all power generation variables have a hat (*e.g.*, \hat{p}_g and \hat{q}_g). Underlining and overlining signify lower and upper bounds, respectively (*e.g.*, $\underline{p}_g^{\text{gen}}$ and $\overline{p}_g^{\text{gen}}$). Additionally, when a parameter or variable name appears in bold, it denotes the vector comprising all the indexed elements (*e.g.*, $\mathbf{x} = [x_{kr}, \forall k \in K, \forall r \in R]$). When necessary, we apply a superscript ω (*e.g.*, ξ^ω) to indicate a quantity associated specifically with scenario ω . All power grid parameters and variables are assumed to be in the per-unit system.

3.2. Resilience Modeling

The discrete set of implementable resilience levels is denoted by R , and the decision to reinforce substation k to a specific level r is captured by the binary decision variable x_{kr} . Substation k is resilient to level r flooding if $x_{kr} = 1$ and is otherwise susceptible. The mitigation model comprises three sets of constraints involving these variables:

$$x_{k,r+1} \leq x_{k,r}, \quad \forall k \in K, \forall r \in R \setminus \{\hat{r}\}, \quad (1)$$

$$x_{k\hat{r}} = 0, \quad \forall k \in K, \quad (2)$$

$$\sum_{k \in K} \sum_{r \in R} c_{kr} x_{kr} \leq f. \quad (3)$$

Constraints (1) capture the cumulative nature of mitigation. We suppose the mitigation is limited either physically or practically and introduce \hat{r} as the unattainable level of resilience. Flooding at or above the unattainable level is rendered inexorable by constraints (2). Finally, we suppose the mitigation resources are limited to a budget of f . Supposing a marginal cost c_{kr} associated with each decision x_{kr} , this is captured by the binary knapsack constraint (3). For brevity, we hereafter refer to the constraints of the mitigation decision making problem as

$$\mathcal{X} = \{\mathbf{x} \in \{0, 1\}^{|K \times R|} : (1), (2), (3)\}. \quad (4)$$

3.3. Power Flow Modeling

Our recourse problems are based on two linear approximations of ACPF: the classical DC approximation (Molzahn and Hiskens 2019) and the more contemporary and fidelitous linear programming AC (LPAC) approximation (Coffrin and Van Hentenryck 2014). In this section, we present adaptations of the models that account for incapacitated substations and incorporate various levels of detail. In each model, we assume that a bus is operational if and only if its substation is operational. Similarly, we assume that a branch is operational if and only if both of its bus endpoints are operational. Because these conditions are subject to change as a result of unpredictable flooding and prior mitigation decision making, each recourse problem is modeled as a function of a specific set of flood mitigation decisions and a specific flooding realization.

3.3.1. AC Power Flow. Both the DC and LPAC approximations are based on the four core ACPF equations:

$$\sum_{g \in G_n} \hat{p}_g - \sum_{d \in D_n} p_n^{\text{load}} = \sum_{l \in L_n} \tilde{p}_l, \quad \forall n \in N, \quad (5)$$

$$\sum_{g \in G_n} \hat{q}_g - \sum_{d \in D_n} q_d^{\text{load}} = \sum_{l \in L_n} \tilde{q}_l, \quad \forall n \in N, \quad (6)$$

$$\tilde{p}_l = v_n^2 g_l - v_n v_m g_l \cos(\theta_n - \theta_m) - v_n v_m b_l \sin(\theta_n - \theta_m), \quad \forall (n, m) \in E, \forall l \in L_{nm}, \quad (7)$$

$$\tilde{q}_l = -v_n^2 b_l + v_n v_m b_l \cos(\theta_n - \theta_m) - v_n v_m g_l \sin(\theta_n - \theta_m), \quad \forall (n, m) \in E, \forall l \in L_{nm}. \quad (8)$$

These equations are based on the simple series admittance model of a branch (Molzahn and Hiskens 2019). Here, complex power is represented in rectangular form (*i.e.*, $p + jq$) and complex voltage in polar form (*i.e.*, $ve^{j\theta}$). Linear equations (5) and (6) capture Kirchhoff's Current Law (KCL), and nonconvex equations (7) and (8) capture Ohm's Law. Many approximation, relaxation, and restriction PF models are obtained by manipulating the nonconvex equations to make them more computationally tractable.

3.3.2. Adapted DC Model. The classical DC approximation is based on three assumptions.

1. Branch conductance is negligible relative to susceptance and may be neglected.
2. Bus voltage magnitudes may be fixed to one per unit.
3. The difference between voltage phase angles of adjacent buses is small such that the sine of that difference may be accurately modeled by the difference itself and the cosine may be fixed to one.

These assumptions lead to the reactive power flows being zero and the active power flows obeying a linear relationship with the bus voltage phase angles. This model may be viewed as an extension of a capacitated network flow problem involving multiple sources and sinks. Importantly, the solution space is additionally confined by the complicating Ohm's Law equality constraints. Our adaptation of the DC approximation is

$$\mathcal{L}_{\text{DC}}(\mathbf{x}, \boldsymbol{\xi}) = \min \lambda^{\text{shed}} \sum_{d \in D} p_d^{\text{load}} (1 - \delta_d) + \lambda^{\text{over}} \sum_{g \in G} \check{p}_g \quad (9a)$$

$$\text{s.t. } \alpha_n = \prod_{r \in R} (1 - \xi_{kr} (1 - x_{kr})), \quad \forall k \in K, \forall n \in N_k, \quad (9b)$$

$$\beta_{nm} = \alpha_n \alpha_m, \quad \forall (n, m) \in E, \quad (9c)$$

$$\delta_d \leq 1 - \chi, \quad \forall d \in D, \quad (9d)$$

$$\begin{aligned} & \sum_{g \in G_n} (\hat{p}_g - \check{p}_g) + \sum_{l \in L_n^+} \tilde{p}_l \\ &= \sum_{d \in D_n} p_d^{\text{load}} \delta_d + \sum_{l \in L_n^-} \tilde{p}_l, \quad \forall n \in N, \end{aligned} \quad (9e)$$

$$M(\beta_{nm} - 1) \leq -\tilde{p}_l - b_l \widehat{\sin}_{nm}, \quad \forall (n, m) \in E, \forall l \in L_{nm}, \quad (9f)$$

$$M(1 - \beta_{nm}) \geq -\tilde{p}_l - b_l \widehat{\sin}_{nm}, \quad \forall (n, m) \in E, \forall l \in L_{nm}, \quad (9g)$$

$$\widehat{\sin}_{nm} \in \mathcal{Y}_{\sin}(\theta_n, \theta_m, \beta_{nm}), \quad \forall (n, m) \in E, \quad (9h)$$

$$-\bar{s}_l^{\text{flow}} \beta_{nm} \leq \tilde{p}_l \leq \bar{s}_l^{\text{flow}} \beta_{nm}, \quad \forall (n, m) \in E, \forall l \in L_{nm}, \quad (9i)$$

$$\underline{p}_g^{\text{gen}}(\alpha_n - \chi) \leq \hat{p}_g \leq \bar{p}_g^{\text{gen}} \alpha_n, \quad \forall n \in N, \forall g \in G_n, \quad (9j)$$

$$\check{p}_g \leq \hat{p}_g, \quad \forall g \in G, \quad (9k)$$

$$\theta_{n_{\text{ref}}} = 0. \quad (9l)$$

Here, variables are also constrained as specified in Section 3.1. The objective (9a) is to minimize the weighted combination of active power load shed and overgeneration. Constraints (9b) and (9c) relate the operational statuses of buses and branches to those of the substations. Note that these are equality constraints. As such, every component's operational status is determined exactly by \mathbf{x} and $\boldsymbol{\xi}$, the arguments to \mathcal{L}_{DC} . The logical formulation here is nonlinear, but linear reformulations are presented in Section 3.3.4. Constraints (9d) ensure that no load is satisfied under a grid-wide blackout. Kirchhoff's Current Law (KCL), the PF equivalent of flow balance, is imposed by constraints (9e). In the standard DC approximation, Ohm's Law is represented as the equality constraint $-p_l - b_l \widehat{\sin} = 0$. To ensure out-of-service branches are treated as open circuits, we embed the big- M technique from Coffrin et al. (2011) in constraints (9f) and (9g) to enforce the equality only for operational branches. Details on how the big- M constants may be calibrated are presented in Section 3.3.6. The approximation of $\sin(\theta_n - \theta_m)$ is captured by constraints (9h). In our implementation,

$$\mathcal{Y}_{\sin}(\theta_n, \theta_m, \beta_{nm}) = \left\{ \widehat{\sin} : \widehat{\sin} = \theta_n - \theta_m, \right. \\ \left. -2(1 - \beta_{nm})\bar{\theta} - \beta_{nm}\bar{\theta}_{\Delta} \leq \widehat{\sin} \leq 2(1 - \beta_{nm})\bar{\theta} + \beta_{nm}\bar{\theta}_{\Delta} \right\}. \quad (10)$$

That is, we model $\sin(\theta_n - \theta_m) \approx \theta_n - \theta_m$ with $\widehat{\sin} \in [-\bar{\theta}_{\Delta}, \bar{\theta}_{\Delta}]$ if $\beta_{nm} = 1$ and $\widehat{\sin} \in [-2\bar{\theta}, 2\bar{\theta}]$ if $\beta_{nm} = 0$ so that both θ_n and θ_m are free to assume any value in their ordinary $[-\bar{\theta}, \bar{\theta}]$ range. Constraints (9i) impose conditional lower and upper bounds on power flows. Power generation lower and upper bounds are imposed by constraints (9j). The bounds depend on the operational status of the corresponding bus and on the blackout indicator variable χ . Section 3.5 provides a more thorough discussion on generator modeling and instance feasibility. Constraints (9k) ensure no more power is thrown away than is generated at each generator, and constraint (9l) ensures the voltage phase angle of the reference bus is exactly zero.

3.3.3. Adapted LPAC Model. Recall one of the assumptions underlying the DC approximation is that bus voltage magnitudes may be set to one per unit. This assumption is reasonable when the grid is in good health, *e.g.*, when determining locational marginal prices (Liu et al. 2009, Paul et al. 2017). However, this assumption is less likely to hold when the grid is stressed by multiple damaged components as is often the case during and after extreme weather events.

In Coffrin and Van Hentenryck (2014), hot-, warm-, and cold-start variants of LPAC are proposed for situations where all, some, or no information about bus voltage magnitudes are available. We leverage the warm-start LPAC approximation which incorporates deviations from target bus voltage magnitudes. This grants some flexibility in the feasible solutions, and stable grid operation is still ensured by bounding the deviations. The warm-start variant additionally incorporates reactive power and line losses. The approximation is based on four assumptions, some the same as for the DC approximation.

1. The difference of adjacent buses' voltage phase angles is small such that the sine of that difference may be accurately modeled by the difference itself.
2. The cosine of adjacent buses' voltage phase angles may be accurately modeled by a polyhedral relaxation of cosine.
3. The effects of bus voltage magnitude deviations on active power flow are negligible.
4. Target bus voltage magnitudes are available, and the effects of bus voltage magnitude deviations on reactive power flow may be modeled by a linear approximation of bus voltage around the target.

The LPAC approximation is developed using variable substitutions, first-order Taylor polynomial approximations, and McCormick envelopes. Just as the DC approximation may be interpreted as a sort of network flow problem, the LPAC approximation may be viewed as a capacitated multi-source, multi-sink, and moreover multi-layer network flow problem in which intra- and inter-network interactions are dictated by the complicating Ohm's Law equality constraints. Our adaptation of this model is

$$\begin{aligned} \mathcal{L}_{\text{LPAC}}(\mathbf{x}, \boldsymbol{\xi}) = \\ \min \quad & \lambda^{\text{shed}} \sum_{d \in D} p_d^{\text{load}} (1 - \delta_d) + \lambda^{\text{over}} \sum_{g \in G} \check{p}_g \end{aligned} \tag{11a}$$

$$\text{s.t.} \quad (9b), (9c), (9d), \tag{11b}$$

$$\sum_{g \in G_n} (\hat{p}_g - \check{p}_g) = \sum_{d \in D_n} p_d^{\text{load}} \delta_d + \sum_{l \in L_n} \tilde{p}_l, \quad \forall n \in N, \quad (11c)$$

$$\sum_{g \in G_n} \hat{q}_g = \sum_{d \in D_n} q_d^{\text{load}} \delta_d + \sum_{l \in L_n} \tilde{q}_l, \quad \forall n \in N, \quad (11d)$$

$$\begin{aligned} M(\beta_{nm} - 1) \leq & -\tilde{p}_l + v_n g_l (v_m - v_n) \chi + v_n^2 g_l \\ & - v_n v_m (g_l \widehat{\cos}_{nm} + b_l \widehat{\sin}_{nm}), \quad \forall (n, m) \in E, \forall l \in L_{nm}, \end{aligned} \quad (11e)$$

$$\begin{aligned} M(1 - \beta_{nm}) \geq & -\tilde{p}_l + v_n g_l (v_m - v_n) \chi + v_n^2 g_l \\ & - v_n v_m (g_l \widehat{\cos}_{nm} + b_l \widehat{\sin}_{nm}), \quad \forall (n, m) \in E, \forall l \in L_{nm}, \end{aligned} \quad (11f)$$

$$\begin{aligned} M(\beta_{nm} - 1) \leq & -\tilde{q}_l + v_n b_l (v_n - v_m) \chi - v_n^2 b_l \\ & - v_n v_m (g_l \widehat{\sin}_{nm} - b_l \widehat{\cos}_{nm}) \\ & - v_n b_l (\phi_n - \phi_m) - (v_n - v_m) b_l \phi_n, \quad \forall (n, m) \in E, \forall l \in L_{nm}, \end{aligned} \quad (11g)$$

$$\begin{aligned} M(1 - \beta_{nm}) \geq & -\tilde{q}_l + v_n b_l (v_n - v_m) \chi - v_n^2 b_l \\ & - v_n v_m (g_l \widehat{\sin}_{nm} - b_l \widehat{\cos}_{nm}) \\ & - v_n b_l (\phi_n - \phi_m) - (v_n - v_m) b_l \phi_n, \quad \forall (n, m) \in E, \forall l \in L_{nm}, \end{aligned} \quad (11h)$$

$$\widehat{\sin}_{nm} \in \mathcal{Y}_{\sin}(\theta_n, \theta_m, \beta_{nm}), \quad \forall (n, m) \in E, \quad (11i)$$

$$\widehat{\cos}_{nm} \in \mathcal{Y}_{\cos}(\theta_n, \theta_m, \beta_{nm}), \quad \forall (n, m) \in E, \quad (11j)$$

$$(\tilde{p}_l, \tilde{q}_l) \in \mathcal{Y}_{\text{disc}}(\beta_{nm}), \quad \forall (n, m) \in E, \forall l \in L_{nm}, \quad (11k)$$

$$\underline{p}_g^{\text{gen}}(\alpha_n - \chi) \leq \hat{p}_g \leq \bar{p}_g^{\text{gen}} \alpha_n, \quad \forall n \in N, \forall g \in G_n, \quad (11l)$$

$$\underline{q}_g^{\text{gen}} \alpha_n \leq \hat{q}_g \leq \bar{q}_g^{\text{gen}} \alpha_n, \quad \forall n \in N, \forall g \in G_n, \quad (11m)$$

$$\check{p}_g \leq \hat{p}_g, \quad \forall g \in G, \quad (11n)$$

$$\underline{v}_n \leq v_n + \phi_n \leq \bar{v}_n, \quad \forall n \in N, \quad (11o)$$

$$\theta_{n_{\text{ref}}} = 0, \quad (11p)$$

$$\phi_{n_{\text{ref}}} = 0. \quad (11q)$$

Here, variables are also constrained as specified in Section 3.1. The objective (11a) and constraints (9b), (9c), and (9d) all serve the same purpose as they did in our adaptation of the DC approximation. Constraints (11c) and (11d) capture KCL by enforcing flow balance for both active and reactive power. Constraints (11c) in this model are similar but not exactly the same as constraints (9e). This is because each branch in the LPAC approximation is modeled by “to” and “from” flow variables, whereas each branch in the DC approximation

is modeled by a single undirected flow variable. Constraints (11i) and (11j) model the sine and cosine of the difference of adjacent bus voltage phase angles, and constraints (11k) capture generally the thermal limit on apparent power flow. Constraints (11e), (11f), (11g), and (11h) collectively enforce Ohm’s Law for operational branches. Generator active and reactive power limits are enforced by (11l) and (11m), and the active power overgeneration limits are enforced by (11n). Constraints (11o) bound deviations from the target bus voltage magnitudes. Lastly, constraints (11p) and (11q) fix the phase angle and magnitude of the reference bus voltage.

For our adapted LPAC model, we develop three variants: a relatively loose linear variant (“LPAC-L”), a relatively tight linear variant (“LPAC-T”), and a convex quadratic variant (“QPAC”). All three variants implement \mathcal{Y}_{\sin} as defined in (10), but \mathcal{Y}_{\cos} and $\mathcal{Y}_{\text{disc}}$ are implemented differently. In Coffrin and Van Hentenryck (2014), polygonal relaxations are proposed as a means of linearizing two-dimensional disc and cosine geometries. Of course, tighter polygons are preferred for maintaining an accurate model, but looser polygons are preferred for keeping the problem tractable. To study this tradeoff, we formulate three variants of the LPAC model by incorporating different forms of $\mathcal{Y}_{\text{disc}}$ and \mathcal{Y}_{\cos} .

In the “LPAC-L” variant, we adopt

$$\mathcal{Y}_{\cos}(\theta_n, \theta_m, \beta_{nm}) = \{\widehat{\cos} : \widehat{\cos} = 1\}, \quad (12)$$

$$\mathcal{Y}_{\text{disc}}(\beta_{nm}) = \left\{ (\tilde{p}, \tilde{q}) : \cos(\hat{\theta})\tilde{p} + \sin(\hat{\theta})\tilde{q} \leq \bar{s}^{\text{flow}}\beta_{nm}, \forall \hat{\theta} \in \Theta_{\text{disc}} \right\} \quad (13)$$

with $\Theta_{\text{disc}} = \{\frac{t\pi}{2}, t = 1, \dots, 4\}$ such that $\mathcal{Y}_{\text{disc}}$ is a square if $\beta_{nm} = 1$ and a set containing only $(0,0)$ if $\beta_{nm} = 0$. This variant is based on one of the assumptions that underlies the DC approximation – the difference of phase angles at adjacent buses is small such that the sine is approximately linear, and the cosine is approximately 1. For the case of $\beta_{nm} = 1$, these geometries are illustrated in the top row of subplots in Figure 2.

Our second, still linear, variant “LPAC-T” incorporates a polygonal relaxation of the disc and cosine. Define

$$\mathcal{B}_1(\theta; \hat{\theta}) = (\hat{\theta} - \theta) \sin(\hat{\theta}) + \cos(\hat{\theta}) \quad (14)$$

as the line tangent to $\cos(\theta)$ at $\hat{\theta}$. In the “LPAC-T” variant, we let

$$\mathcal{Y}_{\cos}(\theta_n, \theta_m, \beta_{nm}) = \left\{ \widehat{\cos} : \widehat{\cos} \leq (1 - \beta_{nm})(1 - \min\{\mathcal{B}_1(-2\bar{\theta}; \hat{\theta}), \mathcal{B}_1(2\bar{\theta}; \hat{\theta})\}) + \mathcal{B}_1(\theta_n - \theta_m; \hat{\theta}), \forall \hat{\theta} \in \Theta_{\cos} \right\} \quad (15)$$

with $\Theta_{\cos} = \{0, \pm 0.354, \pm 0.735, \pm 1.211\}$ such that \mathcal{Y}_{\cos} is a seven-edge polygonal relaxation of cosine when $\beta_{nm} = 1$. When $\beta_{nm} = 0$, the polygon is relaxed so that θ_n and θ_m are free to take values in the $[-\bar{\theta}, \bar{\theta}]$ range and $\widehat{\cos}$, an arbitrary decision variable in that case, is free to take values in $[\cos(\bar{\theta}_{\Delta}), 1]$. This specific Θ_{\cos} is further motivated in Section 3.3.5. The “LPAC-T” variant also incorporates (13) but with $\Theta_{\text{disc}} = \{\frac{t\pi}{6}, t = 1, \dots, 12\}$ such that $\mathcal{Y}_{\text{disc}}$ is a regular dodecahedron. For the case of $\beta_{nm} = 1$, these geometries are illustrated in the middle row of subplots in Figure 2.

Our third variant also retains the linear approximation of sine but employs the exact quadratic model of a disc and the tight convex quadratic relaxation of cosine from Molzahn and Hiskens (2019). In our work, we refer to this variant as the “quadratic programming AC” or “QPAC” variant. Note that “QPAC” is sometimes used to refer to a specific quadratic programming ACPF approximation that was coincidentally patented by some of the same researchers that developed the LPAC approximation (Coffrin and Van Hentenryck 2014, Coffrin et al. 2020), but we do not mean it in that sense. Define

$$\mathcal{B}_2(\theta) = (1 - \cos(\bar{\theta}_{\Delta})) (\theta / \bar{\theta}_{\Delta})^2 \quad (16)$$

as the convex quadratic curve that bounds $\cos(\theta)$ and intersects it at $-\bar{\theta}_{\Delta}, 0$, and $\bar{\theta}_{\Delta}$. Our “QPAC” variant implements

$$\mathcal{Y}_{\cos}(\theta_n, \theta_m, \beta_{nm}) = \{\widehat{\cos} : \widehat{\cos} \leq \mathcal{B}_2(\theta) + (1 - \beta_{nm})(1 - \min\{\mathcal{B}_2(-2\bar{\theta}), \mathcal{B}_2(2\bar{\theta})\})\}, \quad (17)$$

$$\mathcal{Y}_{\text{disc}}(\beta_{nm}) = \{(\tilde{p}, \tilde{q}) : \tilde{p}^2 + \tilde{q}^2 \leq (\bar{s}^{\text{flow}})^2 \beta_{nm}\}. \quad (18)$$

Though this model sacrifices linearity, it allows the disc and cosine geometries to each be modeled using one quadratic inequality constraint (as opposed multiple linear inequality constraints). In the case of $\beta = 0$, these implementations behave the same as those from the “LPAC-T” variant. In the case of $\beta_{nm} = 1$, these geometries are illustrated in the bottom row of subplots in Figure 2.

3.3.4. Linearization of Logical Constraints. In our DC and LPAC adaptations, (9b) and (9c) are logical constraints that relate substation, bus, and branch statuses. These nonlinear constraints, however, admit linear reformulations as detailed in Asghari et al. (2022). We accordingly reformulate constraints (9b) as

$$\alpha_n \geq \sum_{r \in R} (1 - \xi_{kr} (1 - x_{kr})) - |R| + 1, \quad \forall k \in K, \forall n \in N_k, \quad (19a)$$

$$\alpha_n \leq 1 - \xi_{kr} (1 - x_{kr}), \quad \forall k \in K, \forall n \in N_k, \forall r \in R. \quad (19b)$$

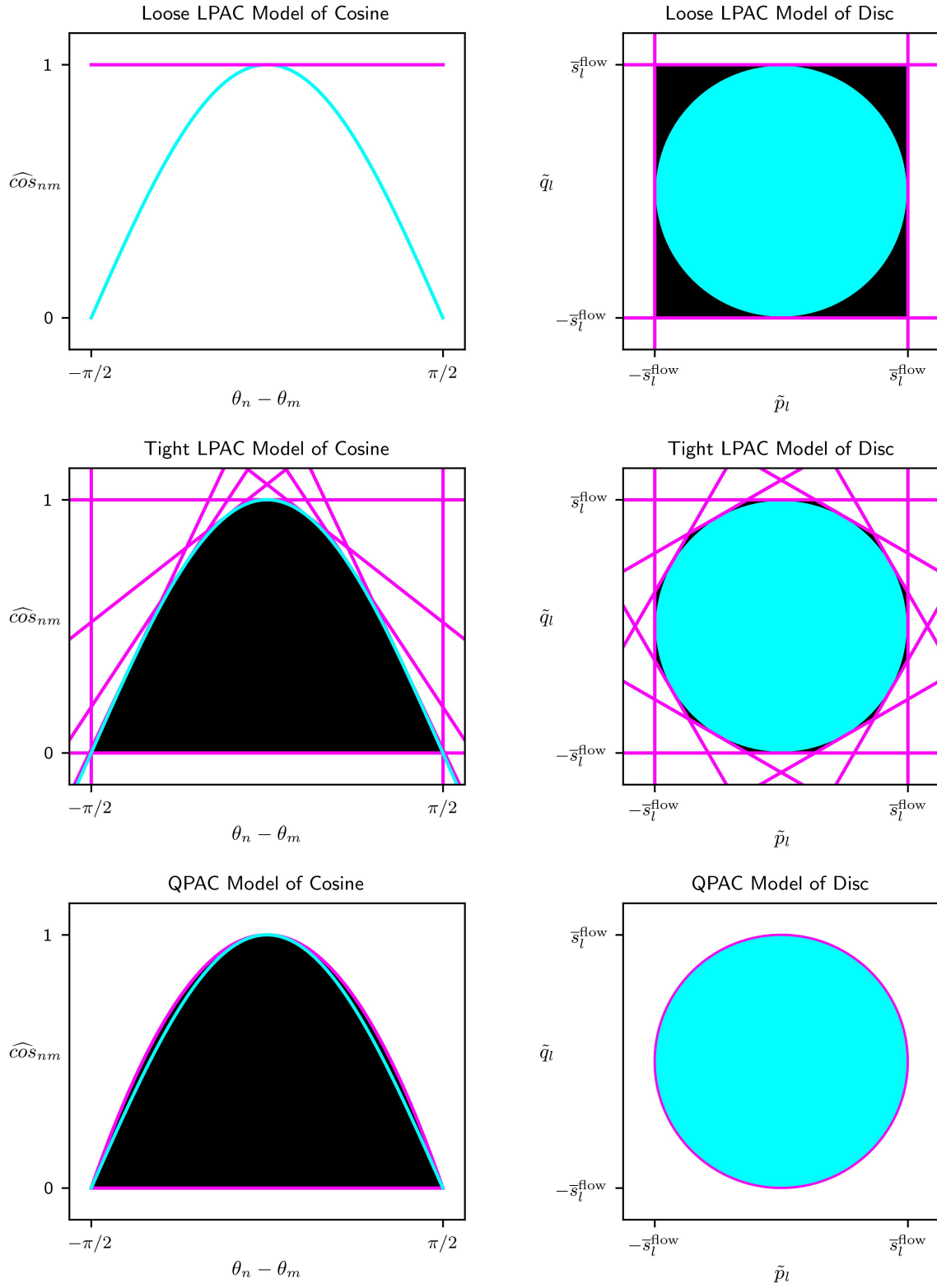


Figure 2 The cosine and disc geometries modeled in our three variants of $\mathcal{L}_{\text{LPAC}}$ in the case of $\beta_{nm} = 1$.

The first set of constraints require that a bus be operational if the associated substation experiences flooding below the implemented resilience level, and the second set requires that a bus not be operational otherwise.

Similarly, constraints (9c) may be reformulated as

$$\beta_{nm} \geq \alpha_n + \alpha_m - 1, \quad \forall (n, m) \in E, \quad (20a)$$

$$\beta_{nm} \leq \alpha_n, \quad \forall (n, m) \in E, \quad (20b)$$

$$\beta_{nm} \leq \alpha_m, \quad \forall (n, m) \in E. \quad (20c)$$

These constraints require that branches along an edge be operational if both bus endpoints of that edge are operational, and that they not be operational if one or both bus endpoints are not operational.

3.3.5. Tightening the Polygonal Relaxation of Cosine. In Coffrin and Van Hentenryck (2014), the proposed polygonal relaxation of cosine is (15) with $\Theta_{\cos} = \left\{ \left(\frac{2t-T-1}{T-1} \right) \bar{\theta}_\Delta, t = 1, \dots, T \right\}$ for some integer number of edges T . This relaxation is such that the tangent lines intersect the cosine curve at points equidistant on the interval $[-\bar{\theta}_\Delta, \bar{\theta}_\Delta]$. A shortcoming of this particular relaxation is that the potential for overestimation error is the greatest in the vicinity of $\theta = \theta_n - \theta_m = 0$ as pictured in the top row of subplots in Figure 3.

Because our approximation of sine is based on the assumption that $\theta_n - \theta_m$ is small, it would be ideal for the relaxation of cosine to be tighter for such values. To remedy this issue, we propose using a Θ_{\cos} that minimizes the worst-case relaxation error. Let $\hat{\theta}$ be a point at which some bounding tangent line intersects $\cos(\theta)$ and let $\Theta_{\cos} = \{\hat{\theta}_1, \dots, \hat{\theta}_T\}$ be a set of T such points. Subject to $-\bar{\theta}_\Delta \leq \hat{\theta}_1 \leq \dots \leq \hat{\theta}_T \leq \bar{\theta}_\Delta$, the set Θ_{\cos} that minimizes the maximum relaxation error is the solution to the following trilevel optimization problem:

$$\min_{\hat{\theta}_1, \dots, \hat{\theta}_T} \max_{-\bar{\theta}_\Delta \leq \theta \leq \bar{\theta}_\Delta} \min_{t=1, \dots, T} \{ \mathcal{B}_1(\theta; \hat{\theta}_t) - \cos(\theta) \}. \quad (21)$$

The outer level is a minimum over the decision variables, the middle level is a maximum over the range of permissible θ , and the inner level simply captures the distance between $\cos(\theta)$ and the nearest bounding tangent line at θ . Note that this problem is independent of the flooding uncertainty. As such, $\hat{\theta}_1, \dots, \hat{\theta}_T$ may be computed by solving (21) once and then applied to each recourse problem's constraints.

Intuitively, the worst-case error of a polygonal relaxation would only occur at one of the points where adjacent tangent lines intersect or at one of the endpoints of the interval $[-\bar{\theta}_\Delta, \bar{\theta}_\Delta]$. This observation allows us to analytically eliminate the inner-level minimum to simplify the formulation. Let $\tilde{\theta}_{t,t+1}$ be the point θ at which $\mathcal{B}_1(\theta; \hat{\theta}_t) = \mathcal{B}_1(\theta; \hat{\theta}_{t+1})$. Analytically,

$$\tilde{\theta}_{t,t+1} = \frac{\hat{\theta}_t \sin(\hat{\theta}_t) - \hat{\theta}_{t+1} \sin(\hat{\theta}_{t+1}) + \cos(\hat{\theta}_t) - \cos(\hat{\theta}_{t+1})}{\sin(\hat{\theta}_t) - \sin(\hat{\theta}_{t+1})}, \quad (22)$$

and

$$\mathcal{B}_1(\tilde{\theta}_{t,t+1}; \hat{\theta}_t) = \frac{\sin(\hat{\theta}_t) \cos(\hat{\theta}_{t+1}) - \cos(\hat{\theta}_t) \sin(\hat{\theta}_{t+1}) - (\theta_t - \theta_{t+1}) \sin(\theta_t) \sin(\theta_{t+1})}{\sin(\hat{\theta}_t) - \sin(\hat{\theta}_{t+1})}. \quad (23)$$

This leads to the bilevel reformulation

$$\min \quad z \quad (24a)$$

$$\text{s.t.} \quad -\bar{\theta}_\Delta \leq \hat{\theta}_1 \leq \dots \leq \hat{\theta}_T \leq \bar{\theta}_\Delta \quad (24b)$$

$$z \geq \mathcal{B}_1(\tilde{\theta}_{t,t+1}; \hat{\theta}_t) - \cos(\tilde{\theta}_{t,t+1}), \quad t = 1, \dots, T-1, \quad (24c)$$

$$z \geq \mathcal{B}_1(-\bar{\theta}_\Delta; \hat{\theta}_1) - \cos(-\bar{\theta}_\Delta), \quad (24d)$$

$$z \geq \mathcal{B}_1(\bar{\theta}_\Delta; \hat{\theta}_T) - \cos(\bar{\theta}_\Delta), \quad (24e)$$

$$(22), (23)$$

in which the second-level maximum is modeled using the variable z . This model still involves many trigonometric functions and is accordingly nonconvex. We solve the model for $|\Theta_{\cos}| = 5$ and $|\Theta_{\cos}| = 7$ and for $\bar{\theta}_\Delta = \frac{\pi}{2}$ using the Knitro solver (Byrd et al. 2006) available through the Network-Enabled Optimization Solver (NEOS) Server (Czyzyk et al. 1998, Dolan 2001, Gropp and Moré 1997). For these parameters, the differences between Θ_{\cos} being composed of equidistant points versus points spaced as prescribed by our optimization model are illustrated in Figure 3. We use the set comprising 7 points in our LPAC-T variant.

3.3.6. Tightening the Ohm's Law Constraints. In the original DC and LPAC approximations, Ohm's Law applies to all branches unconditionally because all branches are assumed to be operational. To account for substation damages and resilience decisions, both our adapted DC and LPAC models account for the status of each bus and branch by an indicator variable. Because branch status is a variable in our adaptations, we use the big- M modeling technique to only enforce Ohm's Law for operational branches. Unfortunately, this technique

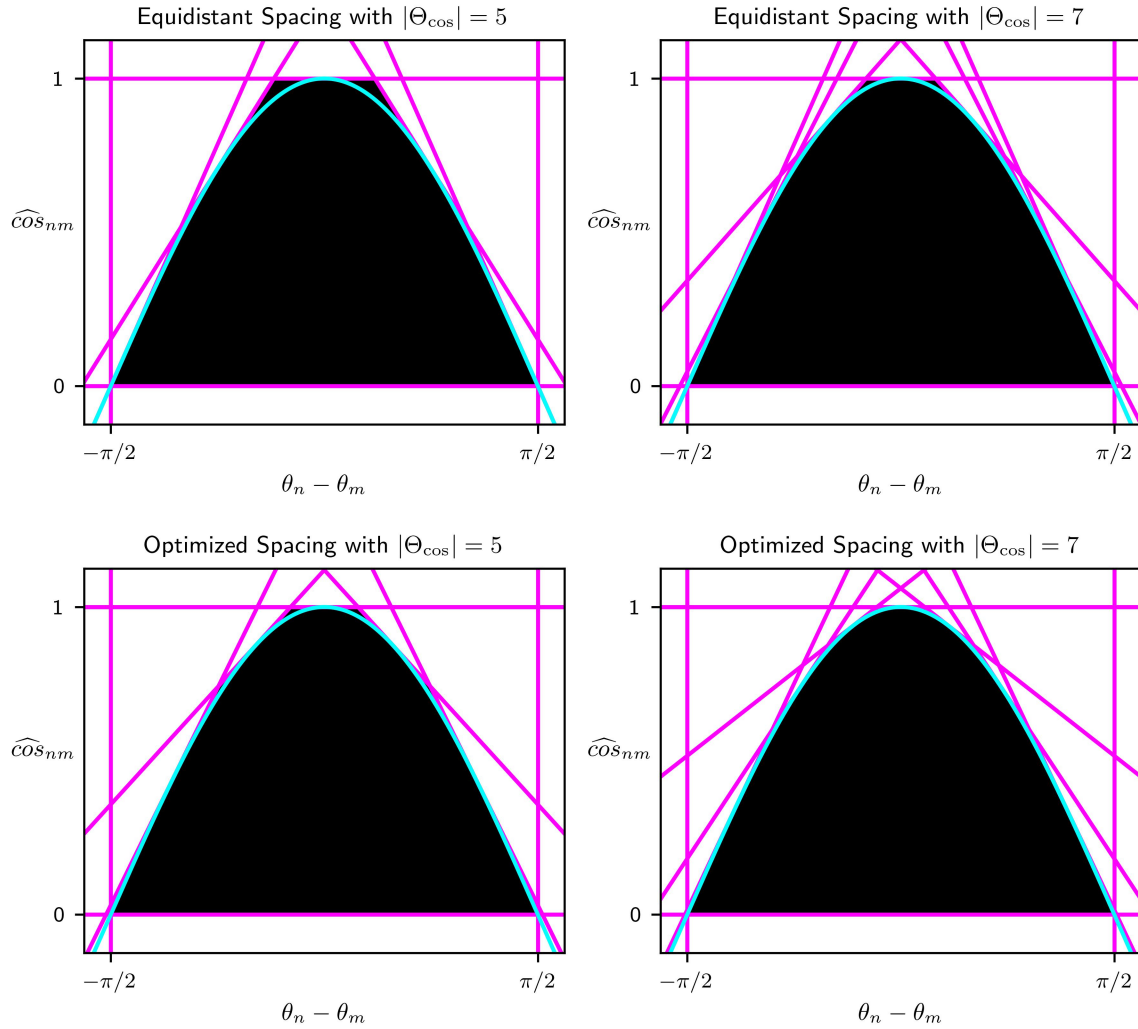


Figure 3 A comparison of the polygonal relaxations of cosine with equally (top row) and optimally (bottom row) spaced tangent line intersection points for $|\Theta_{\cos}| = 5$ and $|\Theta_{\cos}| = 7$.

can require careful calibration of the big- M constants. Having big- M constants that are too large may cause the solution space of the linear programming (LP) relaxation to be loose relative to the convex hull of the integer-feasible solution space, and this can affect the bound provided by the LP relaxations in mixed-integer algorithms like branch-and-bound. It is possible to calibrate these constants to make the constraints tight. In this section, we present the optimization problems for determining well-calibrated big- M constants in our model. The idea is to find the minimum or maximum value of the right-hand side of each Ohm's Law constraint in the case of $\beta_{nm} = 0$ (*i.e.*, the case when the big- M constant takes effect).

For the DC adaptation, the optimization problems for determining the big- M constants are

$$\begin{aligned} M_{n,m,l}^{(9f)} = \min \quad & -b_l \widehat{\sin}_{nm} \\ \text{s.t.} \quad & \widehat{\sin} \in \mathcal{Y}_{\sin}(\theta_n, \theta_m, 0), \end{aligned} \quad (25)$$

$$\begin{aligned} M_{n,m,l}^{(9g)} = \max \quad & -b_l \widehat{\sin}_{nm} \\ \text{s.t.} \quad & \widehat{\sin} \in \mathcal{Y}_{\sin}(\theta_n, \theta_m, 0) \end{aligned} \quad (26)$$

for all $(n, m) \in E, l \in L_{nm}$. The superscript on each big- M denotes the constraint for which the constant is applicable. Note that \tilde{p}_l is absent from the objective function since constraints (11k) restrict it to zero in the case of $\beta_{nm} = 0$.

For the LPAC adaptation, the optimization problems that determine the best constants for the four sets of Ohm's Law constraints are

$$\begin{aligned} M_{n,m,l}^{(11e)} = \min \quad & v_n g_l (v_m - v_n) \chi + v_n^2 g_l - v_n v_m \left(g_l \widehat{\cos}_{n,m} + b_l \widehat{\sin}_{n,m} \right) \\ \text{s.t.} \quad & \widehat{\sin}_{nm} \in \mathcal{Y}_{\sin}(\theta_n, \theta_m, 0), \widehat{\cos}_{nm} \in \mathcal{Y}_{\cos}(\theta_n, \theta_m, 0), \end{aligned} \quad (27)$$

$$\begin{aligned} M_{n,m,l}^{(11f)} = \max \quad & v_n g_l (v_m - v_n) \chi + v_n^2 g_l - v_n v_m \left(g_l \widehat{\cos}_{n,m} + b_l \widehat{\sin}_{n,m} \right) \\ \text{s.t.} \quad & \widehat{\sin}_{nm} \in \mathcal{Y}_{\sin}(\theta_n, \theta_m, 0), \widehat{\cos}_{nm} \in \mathcal{Y}_{\cos}(\theta_n, \theta_m, 0), \end{aligned} \quad (28)$$

$$\begin{aligned} M_{n,m,l}^{(11g)} = \min \quad & v_n b_l (v_n - v_m) \chi - v_n^2 b_l - v_n v_m \left(g_l \widehat{\sin}_{n,m} - b_l \widehat{\cos}_{n,m} \right) \\ & - v_n b_l (\phi_n - \phi_m) - (v_n - v_m) b_l \phi_n^\omega \\ \text{s.t.} \quad & \widehat{\sin}_{nm} \in \mathcal{Y}_{\sin}(\theta_n, \theta_m, 0), \widehat{\cos}_{nm} \in \mathcal{Y}_{\cos}(\theta_n, \theta_m, 0), \\ & \underline{v}_n \leq v_n + \phi_n^\omega \leq \bar{v}_n, \underline{v}_m \leq v_m + \phi_m^\omega \leq \bar{v}_m, \end{aligned} \quad (29)$$

$$\begin{aligned} M_{n,m,l}^{(11h)} = \max \quad & v_n b_l (v_n - v_m) \chi - v_n^2 b_l - v_n v_m \left(g_l \widehat{\sin}_{n,m} - b_l \widehat{\cos}_{n,m} \right) \\ & - v_n b_l (\phi_n - \phi_m) - (v_n - v_m) b_l \phi_n^\omega \\ \text{s.t.} \quad & \widehat{\sin}_{nm} \in \mathcal{Y}_{\sin}(\theta_n, \theta_m, 0), \widehat{\cos}_{nm} \in \mathcal{Y}_{\cos}(\theta_n, \theta_m, 0), \\ & \underline{v}_n \leq v_n + \phi_n^\omega \leq \bar{v}_n, \underline{v}_m \leq v_m + \phi_m^\omega \leq \bar{v}_m. \end{aligned} \quad (30)$$

By design, the linear approximation of sine that we use in all four of models allows $\widehat{\sin}_{nm} \in [-2\bar{\theta}, 2\bar{\theta}]$ independent of θ_n and θ_m when $\beta_{nm} = 0$. Also by design, $\widehat{\cos}_{nm} = 1$ in the LPAC-L model and $\widehat{\cos}_{nm} \in [\cos(\bar{\theta}_\Delta), 1]$ when $\beta_{nm} = 0$ in the LPAC-T and QPAC models independent of θ_n and θ_m . The other variables in these linear big- M optimization problems are all independently constrained, so these problems may be solved easily by optimizing each variable independently.

3.4. Two-Stage Models

Having discussed the resilience and PF models, we now introduce our two-stage models. The first model seeks to minimize the expected load shed. We refer to it as the “Stochastic Programming” (SP) model, and it is formulated as

$$\min_{\mathbf{x} \in \mathcal{X}} \sum_{\omega \in \Omega} \Pr(\omega) \mathcal{L}(\mathbf{x}, \boldsymbol{\xi}^\omega). \quad (\text{SP})$$

Here, \mathcal{X} is as defined in (4) and \mathcal{L} is either (9) or any variant of (11). In this model, the idea is to make first-stage resilience decisions with knowledge of how well the power grid will be able to perform in the aftermath of the hurricane flooding given those decisions. This model adopts the “nature is fair” approach – each scenario ω is believed to occur with probability $\Pr(\omega)$ and is weighted accordingly in the objective function.

Closely related to the SP model are a few solutions and bounds of theoretical and practical importance: the “Expected Value” (EV) solution, the “Expected result of using the Expected Value solution” (EEV) bound, and the “Expected Wait-and-See” (EWS) bound (Birge and Louveaux 2011). An EV solution is obtained by solving a variant of the SP model in which the uncertainty is aggregated to its mean and is defined as

$$\bar{\mathbf{x}} \in \arg \min_{\mathbf{x} \in \mathcal{X}} \mathcal{L}(\mathbf{x}, \bar{\boldsymbol{\xi}}). \quad (\text{EV})$$

For each scenario in the SP model, $\boldsymbol{\xi}^\omega = \mathcal{C}(\boldsymbol{\nu}^\omega)$ where $\mathcal{C} : \mathbb{R}_+^{|K|} \rightarrow \{0, 1\}^{|K \times R|}$ is a function that converts a real-valued vector $\boldsymbol{\nu}^\omega$ of flood levels to a vector $\boldsymbol{\xi}^\omega$ of flood indicators. In (EV) above, $\bar{\boldsymbol{\xi}} = \mathcal{C}(\bar{\boldsymbol{\nu}})$ where $\bar{\boldsymbol{\nu}} = \sum_{\omega \in \Omega} \Pr(\omega) \boldsymbol{\nu}^\omega$. That is, our notion of the mean scenario is the set of flood indicators corresponding to the mean flood levels. The EEV bound is a function of the EV solution:

$$\sum_{\omega \in \Omega} \Pr(\omega) \mathcal{L}(\bar{\mathbf{x}}, \boldsymbol{\xi}^\omega). \quad (\text{EEV})$$

The EEV bound captures how one would fare if one planned for the uncertainty’s mean rather than its probability distribution. It is formulated as a restriction of the SP model that fixes the first-stage solution to an EV solution; thus, the EEV bound is an upper bound on the objective value of the SP model. The difference between the EEV bound and the objective value of the SP model is the “Value of the Stochastic Solution” (VSS).

Moving on, the EWS bound is formulated similarly to the SP model but rather lets the first-stage decisions \mathbf{x} be postponed until after the uncertainty is realized. It is formulated as

$$\sum_{\omega \in \Omega} \Pr(\omega) \min_{\mathbf{x} \in \mathcal{X}} \mathcal{L}(\mathbf{x}, \boldsymbol{\xi}^\omega). \quad (\text{EWS})$$

Consider that the SP model may be equivalently formulated by duplicating the \mathbf{x} variables in each scenario and forcing the duplicate variables to be equal via non-anticipativity constraints. The EWS bound is formulated as the relaxation of the SP model that omits the nonanticipativity constraints. Thus, the EWS bound is a lower bound on the objective value of the SP model. The difference between the objective value of the SP model and the EWS bound is the “Expected Value of Perfect Information” (EVPI).

To contrast the SP model, we also propose a “Robust Optimization” (RO) model:

$$\min_{\mathbf{x} \in \mathcal{X}} \max_{\omega \in \Omega} \mathcal{L}(\mathbf{x}, \boldsymbol{\xi}^\omega). \quad (\text{RO})$$

This model is much the same as the SP model, but it instead adopts the “nature is adversarial” approach. The probability of each scenario, if that information is even available, is ignored. Instead, the associated perspective is that the uncertainty realization will be that which does the most harm given the first-stage resilience decisions. This approach is often seen as overly if not impractically conservative. However, it is still valuable when scenario probabilities are not known or when the impact of one scenario dwarfs those of all other scenarios.

To accompany the RO model, we develop mathematical analogues to the EV solution, EEV bound, and EWS bound that we dub the “Maximum Value” (MV) solution, “Maximum result of the Maximum Value solution” (MMV) bound, and the “Maximum Wait-and-See” (MWS) bound. An MV solution is obtained by solving a variant of the RO model in which the uncertainty is aggregated to the substation-wise maximum and is defined as

$$\hat{\mathbf{x}} \in \min_{\mathbf{x} \in \mathcal{X}} \mathcal{L}(\mathbf{x}, \hat{\boldsymbol{\xi}}). \quad (\text{MV})$$

Here, $\hat{\boldsymbol{\xi}} = \mathcal{C}(\hat{\boldsymbol{\nu}})$ where $\hat{\boldsymbol{\nu}} = \max_{\omega \in \Omega} \boldsymbol{\nu}^\omega$. That is, $\hat{\boldsymbol{\nu}}$ is the scenario in which each substation experiences the worst flooding across any of the original scenarios, and we define the maximum value scenario as the corresponding set of flood indicators. Just as the RO model is a conservative approach to dealing with uncertainty, the MV solution is based on a conservative approach to constructing an aggregate scenario.

Naturally, the MMV bound then captures how one would fare in the RO model if one planned only for the maximum value scenario. Just like the EEV bound is formulated as a restriction of the SP model, the MMV bound is formulated as a restriction of the RO model and thus serves as an upper bound:

$$\max_{\omega \in \Omega} \mathcal{L}(\hat{\mathbf{x}}, \boldsymbol{\xi}^\omega). \quad (\text{MMV})$$

Lastly, the MWS bound is formulated similarly to the RO model but rather lets the first-stage decisions \mathbf{x} be postponed until after the uncertainty is realized. It is formulated as

$$\max_{\omega \in \Omega} \min_{\mathbf{x} \in \mathcal{X}} \mathcal{L}(\mathbf{x}, \boldsymbol{\xi}^\omega). \quad (\text{MWS})$$

In the same way that the EWS bound is formulated as a relaxation of the SP model, the MWS bound is formulated as a relaxation of the RO model and thus serves as a lower bound.

Because the RO model is agnostic to the probability distribution of the scenarios (if one even exists), the mathematical analogues of the VSS and EVPI are not philosophically consistent with the perspective that nature is adversarial. As such, the MMV bound ought to be viewed simply as the performance that results from implementing $\hat{\mathbf{x}}$. Similarly, the MWS bound ought to be viewed simply as a computationally inexpensive lower bound on the RO model’s objective value. Such a bound is useful as it allows one to quickly, though crudely, gauge if a mitigation solution is nearly optimal without having to actually solve the RO model.

3.5. Relatively Complete Recourse

When analyzing power grid contingencies using a PF model, it can occur that the model does not admit a feasible solution for certain contingencies. This is particularly troublesome for two-stage models like the SP and RO models because infeasibility in one or more scenarios causes the entire two-stage model to be infeasible. We design our adaptations of the DC and LPAC models with careful consideration of their role as recourse models in our two-stage formulations, and make certain modeling decisions to ensure their feasibility. Mainly, we incorporate a more relaxed model of generator active power injections than is often used and also introduce a blackout indicator variable that grants relatively complete recourse (Birge and Louveaux 2011) by admitting a trivial blackout solution when no non-trivial solution is feasible.

Table 1 A feasible blackout solution to the recourse problem.

Variable Name	DC Model	LPAC Model	Blackout Value
χ	✓	✓	1
α_n	✓	✓	per (9b)
β_{nm}	✓	✓	per (9c)
δ_d	✓	✓	0
\hat{p}_g	✓	✓	0
\hat{q}_g		✓	0
\check{p}_g	✓	✓	0
\tilde{p}_l	✓	✓	0
\tilde{q}_l		✓	0
$\widehat{\sin}_{nm}$	✓	✓	0
$\widehat{\cos}_{nm}$		✓	1
θ_n	✓	✓	0
ϕ_n		✓	0

In PF models, it is typical to model active power generation limits for a generator g as

$$\underline{p}_g^{\text{gen}} \leq \hat{p}_g \leq \bar{p}_g^{\text{gen}}, \quad (31)$$

with $\underline{p}_g^{\text{gen}}$ and \bar{p}_g^{gen} both strictly positive. In our model of how flooding affects substations, this can easily lead to infeasibility. Suppose there exists a substation with one bus and that the bus has one generator and no load. If that bus is unaffected by flooding but all neighboring substations are affected, then the generator at the bus of the orphaned substation would have nowhere to send the strictly positive amount of power it is required to generate.

To avoid this infeasibility in a computationally tractable way, we still require each generator to produce active power within its lower and upper bounds, but we allow some or all of that power to be discarded at the point of generation. This effectively lowers the generator's lower active power bound to zero. The discarded power or overgeneration at a generator g is a continuous variable denoted \check{p}_g , and we incorporate the overgeneration variables into the objective to keep their values at a minimum.

Other aspects of the original DC and LPAC approximations may also induce infeasibility. To address this broadly, we integrate an indicator variable χ into our adaptations in a way that $\mathcal{L}(\mathbf{x}, \boldsymbol{\xi})$ has relatively complete recourse. Our adapted models are designed such that the variable values detailed in Table 1 are always feasible.

We refer to this solution as the “blackout solution” as it has zero power generation, zero power flow, and zero load satisfied. One can readily verify the feasibility of this solution in our adapted DC model and all three variants of our adapted LPAC model. By design,

the objective value yielded by the blackout solution is $\sum_{d \in D} p_d^{\text{load}}$. There may be other feasible solutions having $\chi = 1$, but the blackout solution is always optimal in this case. From constraints (9d), $\chi = 1 \implies \delta_d = 0, \forall d \in D$. Ergo, the first term in the objective must be $\sum_{d \in D} p_d^{\text{load}}$ in any optimal solution involving $\chi = 1$. Additionally, having $\chi = 1$ reduces the effective lower bounds on active power generation to zero in constraints (9j) from the DC model and constraints (111) from the LPAC model. As such, there is no need for overgeneration, and the second term in the objective function must be zero in any optimal solution involving $\chi = 1$.

Ultimately, recourse models (9) and (11) are designed to admit a non-trivial PF solution with partial or full load satisfaction if such a solution exists and otherwise admit the blackout solution. This allows us to evaluate flooding scenarios of any severity without fear of the overarching two-stage model becoming infeasible. It also grants us the ability to effectively warmstart a solver with any feasible first-stage solution $\mathbf{x} \in \mathcal{X}$.

4. Results

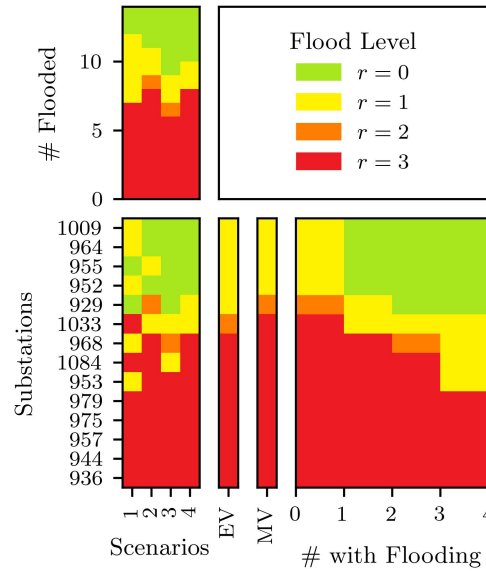
In this section, we describe the case studies we used and the experiments we executed to draw comparisons between the various adaptations of the DC and LPAC approximations that we defined in Section 3 as well as the (SP) and (RO) models. We then assess the optimal objective value and mitigation solution data we obtained.

4.1. Case Studies

We leverage two flooding case studies we developed in past work (Austgen et al. 2023). The first is based on Tropical Storm Imelda from 2019 and the second on Hurricane Harvey from 2017. These events both affected the Texas coastal region, especially Houston, and were noteworthy for their high volumes of precipitation (Blake and Zelinsky 2018, Latta and Berg 2020). Both case studies incorporate a reduction of the ACTIVS 2000-bus synthetic grid of Texas comprising 663 buses near the Texas coast. All PF model parameters are provided by these case studies. We let the unattainable level of resilience be $\hat{r} = 3$. In these case studies, the marginal resource costs of mitigation are assumed to be increasing. Moreover, substations are partitioned into small, medium, and large categories based on the highest-voltage component. Marginal resource costs (*i.e.*, each c_{kr}) for various substation sizes and levels of mitigation are summarized in Table 2.

Table 2 Marginal resource requirements for protecting substations of different sizes.

Highest-Voltage Component	Resilience Level		
	$r = 1$	$r = 2$	$r = 3$
115 kV or 161 kV	1	2	3
230 kV	2	4	6
500 kV	3	6	9

**Figure 4** Tropical Storm Imelda flood levels by scenario and by substation.

Additionally, the Imelda and Harvey case studies respectively comprise 4 and 25 equiprobable scenarios. The flood level indicators for these scenarios as well as the EV and MV scenarios are illustrated in Figures 4 and 5.

4.2. Experiments and Budget Thresholds

We applied each two-stage model from Section 3.4 to the Tropical Storm Imelda and Hurricane Harvey case studies while varying the resource budget f to be integer values between zero and the model's budget threshold (*i.e.*, the maximum useful budget) from Table 3. For the Tropical Storm Imelda case study, we performed these experiments incorporating each of the adapted DC, LPAC-L, LPAC-T, and QPAC models defined in Section 3.3. The Hurricane Harvey case study comprises a greater number of scenarios that affect a larger number of substations as compared to the Imelda case study and thus presented a more difficult computational challenge. To compensate, we only incorporated the adapted DC and LPAC-L models to the Harvey-based instances. We implemented all models in Python using the `gurobipy` package and solved the instances by running the Gurobi solver (Gurobi Optimization, LLC 2022) on 48-core SKX compute nodes from the Stampede2 cluster at the

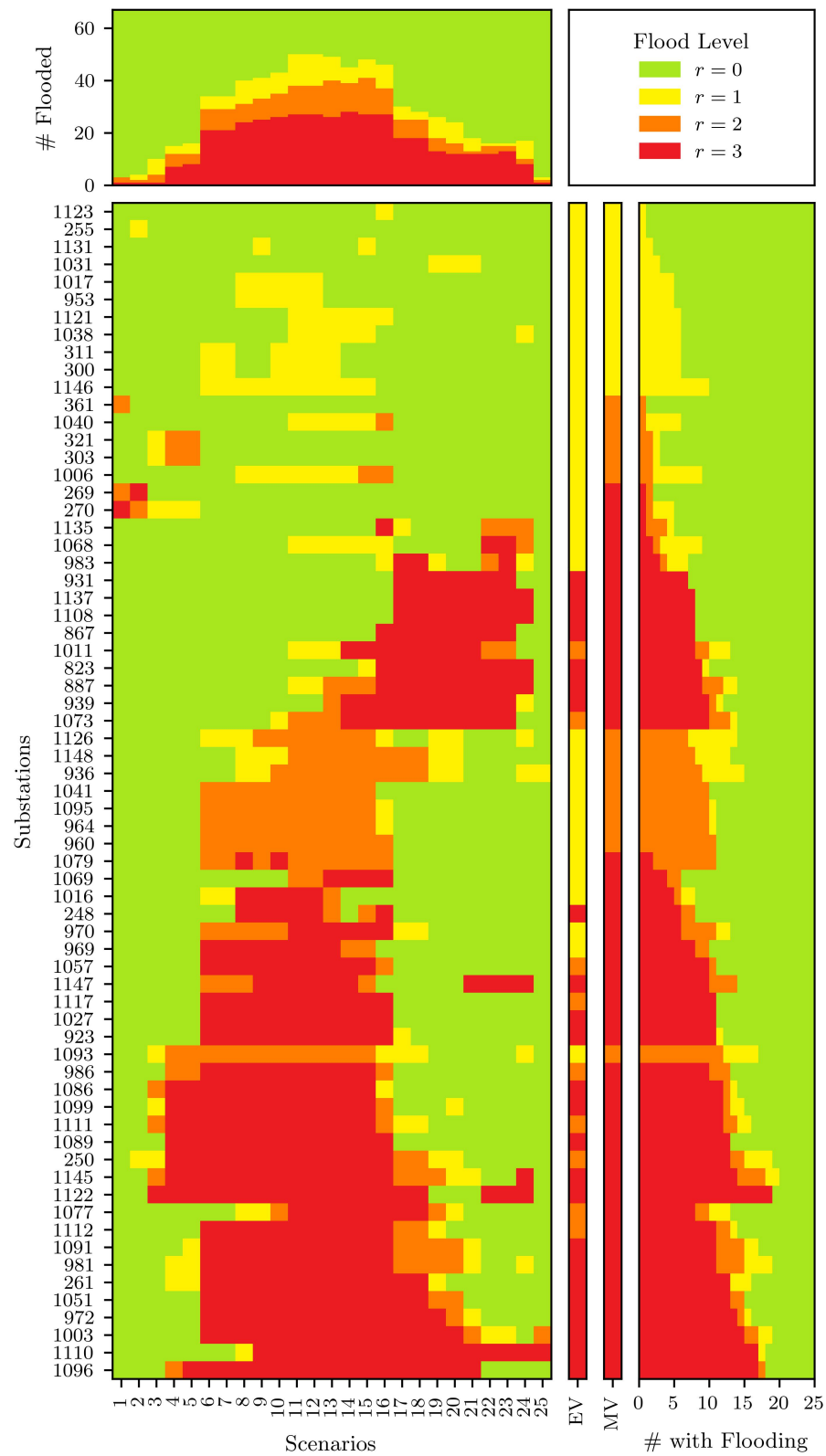


Figure 5 Hurricane Harvey flood levels by scenario and by substation.

Table 3 A summary of the two-stage models/bounds, power flow models, case studies, and budget thresholds in our experiments.

		Case Study	
		Imelda	Harvey
Two-Stage Model/Bound	EEV	9	66
	SP	20	193
	EWS	11	66
	MMV	8	62
	RO	*9	*62
	MWS	*5	*48
Power Flow Model	DC	✓	✓
	LPAC-L	✓	✓
	LPAC-T	✓	
	QPAC	✓	

Texas Advanced Computing Center. We have packaged the input data, code, and result data in a public GitLab repository ([link](#)).

The resource budget thresholds defined in Table 3 are the number of resources that may be effectively used to prevent flooding in each of the two-stage models. Most of these values may be determined prior to solving the associated two-stage model simply by assessing the set of flooding scenarios and the resource costs of the possible mitigation actions. The two exceptions are the budgets for the RO model and MWS bound since the worst-case scenario is not known *a priori* but is rather a function of mitigation decision making such that the threshold may only be determined through optimization. These values are preceded by an asterisk in Table 3. While the thresholds for the RO model and MWS bound could differ based on the chosen PF model, we found them to be the same. To minimize verbosity, we use \bar{f}_X throughout this section to denote the budget threshold for model X.

Recall that some flooding in our model is deemed inexorable via constraints (2). The flooding in the MV scenario is necessarily worse than the flooding in the EV scenario, so the MV scenario has at least as much inexorable flooding. Because the threshold is based on resources used to effectively prevent flooding, it is possible for MMV bound’s budget threshold to be less than the EEV bound’s threshold. Additionally, because these thresholds are easily computed prior to optimization, we only had to compute the EV and MV solutions for integer budgets between 0 and the corresponding threshold. For budgets above the threshold, we avoided the arbitrary deployment of mitigation resources by simply adopting the solution corresponding to the budget threshold. The practical implication of our handling the budget threshold in this way is that the EEV and MMV bounds stagnate for budgets above

the threshold. We also adopted this treatment of the budget threshold for the independent subproblems that must be solved to compute the EWS and MWS bounds.

4.3. Objective Value and Bounds

We study the objective values of the two-stage models mainly to assess the tradeoff between the resource budget and the achievable load shed. The objective values are also useful for comparing the effect of using different PF models, evaluating the tightness of the bounds on the SP and RO models, and computing quantities of theoretical interest like VSS and EVPI. Figures 6 and 7 show the objective value data for the Imelda and Harvey case studies, respectively. We let z_X^* denote the optimal objective value of model X.

As expected, z_{SP}^* and z_{RO}^* monotonically decrease in the budget f . This is a theoretical guarantee since increasing f enlarges the solution space thus allowing better mitigation strategies. For the same reason, z_{EWS}^* and z_{MWS}^* are also monotonic. Because z_{EEV}^* and z_{MMV}^* are based on evaluations of fixed first-stage solutions, these bounds are not monotonically decreasing in f , though they are generally decreasing. Both z_{SP}^* and z_{RO}^* initially make steady improvements as the budget increases from zero, though the marginal improvements granted by additional resources are generally decreasing. In both case studies, z_{EEV}^* and z_{EWS}^* are poor bounds on z_{SP}^* compared to how well z_{MMV}^* and z_{MWS}^* bound z_{RO}^* .

For Imelda, Figure 6 shows that $\bar{f}_{SP} = 20$ Tiger DamsTM up to one meter tall are able to reduce expected load shed (*i.e.*, z_{SP}^*) by 31.6% compared to the “do-nothing” solution. The worst-case load shed (*i.e.*, z_{RO}^*) may be reduced by 42.3% when $\bar{f}_{RO} = 9$ such Tiger DamsTM are deployed. For Harvey, Figure 7 shows improvements of 43.2% and 28.5%, respectively, when $\bar{f}_{SP} = 193$ or $\bar{f}_{RO} = 62$ Tiger DamsTM are deployed.

The bounds in the Imelda case study are tighter than those in the Harvey case study. This is reasonably explained by each ξ^ω for $\omega \in \Omega$ being similar to the others and also to $\bar{\xi}$ and $\hat{\xi}$. This leads to the first-stage decisions in the EV solution and optimal solutions to the SP model and EWS bound subproblems all being similar to one another, and the same is true for the MV solution and optimal solutions to the RO model and MWS bound subproblems.

In both case studies, the VSS (*i.e.*, $z_{EEV}^* - z_{SP}^*$) is generally increasing in the budget and largest when the budget is near \bar{f}_{SP} . That is, the SP model is more valuable for planning with larger budgets than for smaller budgets. The size of the gap also indicates that planning for the expected flooding scenario is a poor strategy, especially for larger budgets. In contrast, the EVPI (*i.e.*, $z_{SP}^* - z_{EWS}^*$) rapidly increases from zero then steadily decreases to zero as the

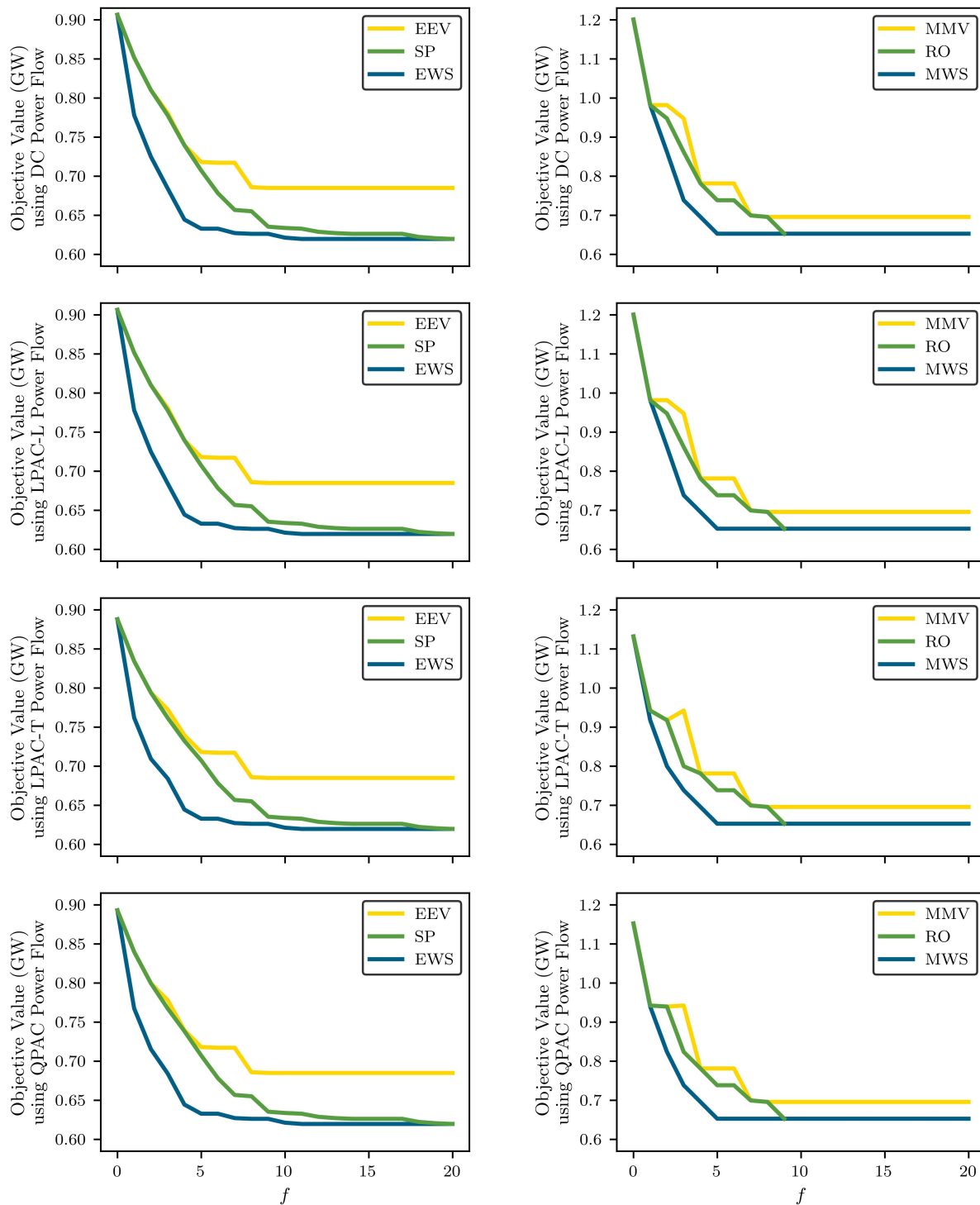


Figure 6 The objective values of the SP and RO models and their bounds in the Tropical Storm Imelda case study.

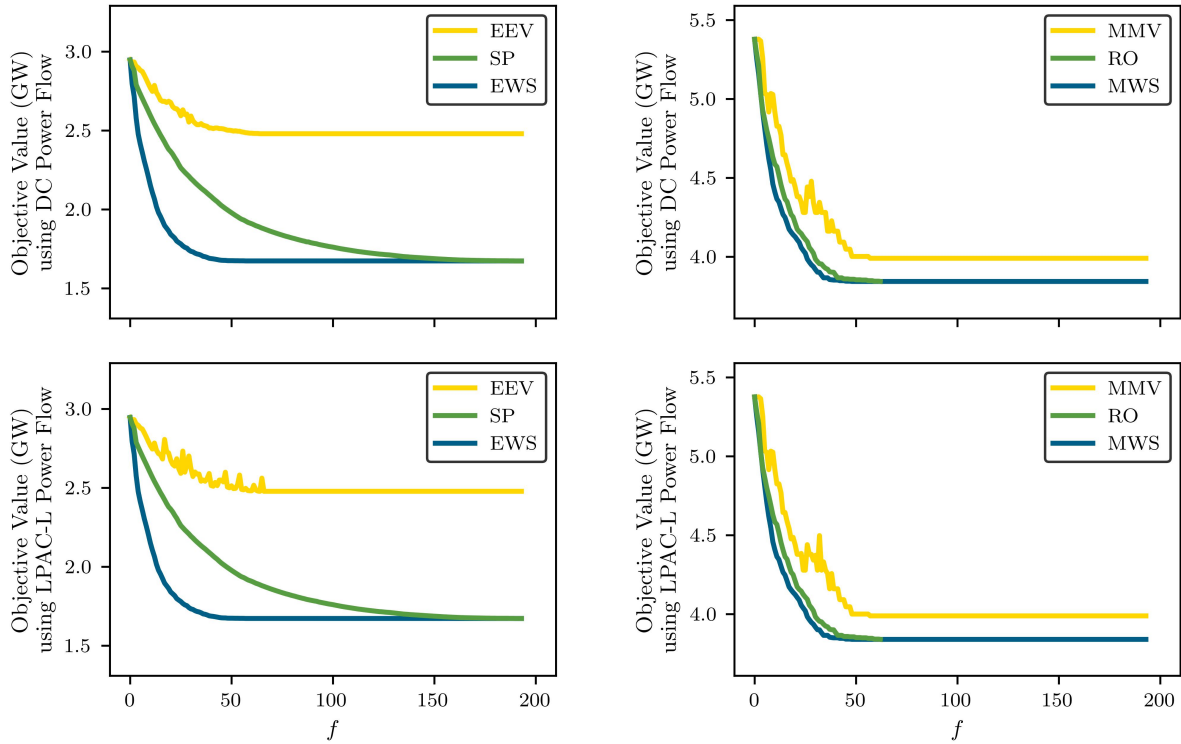


Figure 7 The objective values of the SP and RO models and their bounds in the Hurricane Harvey case study.

budget increases. Specifically, EVPI is largest for budgets roughly halfway between zero and \bar{f}_{EWS} . Intuitively, budgets near the halfway mark are small enough that the marginal return on investment is still substantial and large enough that the variation in flooding scenarios may be more effectively addressed by nuanced decision making. For the RO model, $z_{\text{MMV}}^* - z_{\text{RO}}^*$ is largest for budgets roughly halfway between zero, and \bar{f}_{MMV} , and $z_{\text{RO}}^* - z_{\text{MWS}}^*$ is largest roughly halfway between zero and \bar{f}_{MWS} . Though the reason for the former phenomenon is difficult to determine, the reason for the latter is conceivably the same as for the EVPI.

For the Imelda case study, the time required by the solver to identify a solution and prove its optimality, henceforth referred to as the “time to optimal solution,” was not affected much by the resource budget f as indicated in Figure 8, and all instances solve in a short time. The time to optimal solution for Harvey-based instances, however, was more dependent on f . For example, the times for the SP model with LPAC-L increased from roughly 2 minutes for $f = 0$ to nearly 5 hours for $f = 97$.

For both the SP and RO models, the time to optimal solution tended to peak for budgets roughly halfway between 0 and \bar{f}_{SP} or 0 and \bar{f}_{RO} , respectively. If the budget constraint (3) were an *equality*, then instances with the largest combinatorial decision space, and thus the

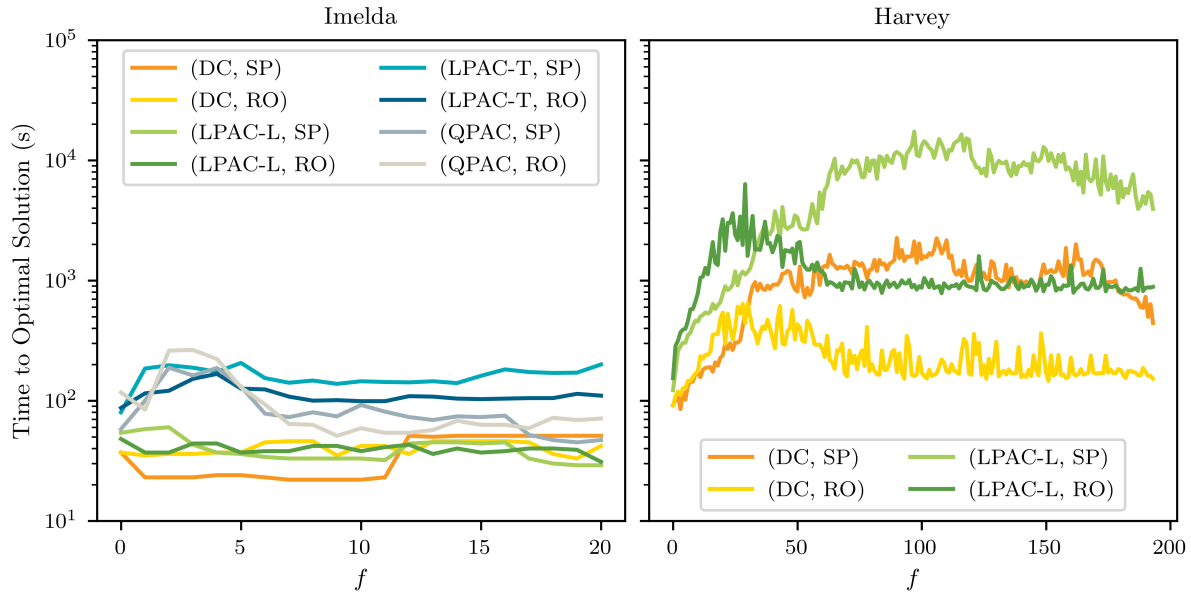


Figure 8 Times required to solve each instance to optimality.

most difficult to solve, would be those with the budget in this vicinity. The budget constraint is actually an *inequality* so the size of the combinatorial decision space is strictly increasing in f . However, because there is an incentive for this constraint to be satisfied at or near equality, solutions using a small portion of the budget are readily fathomed by the solver such that the basic idea holds true.

Lastly, differences induced by the various power models are subtle as shown in Figures 6 and 7. We attribute this to the fact that the PF models all share the same core constraints (*i.e.*, KCL and an approximation of Ohm's Law) and are only subtly different themselves. No matter, while properties like the VSS and EVPI and the effect of the budget on the objective value are of direct interest, objective value differences induced by the chosen PF model only indicate that we should assess the mitigation solutions more qualitatively.

4.4. Mitigation Decisions

The mitigation decisions are the most important decisions in our model and the other decisions serve mainly to capture the operational recourse that influences the mitigation decisions. The operational decisions are for a proxy of ACPF, and the realized flooding is unlikely to exactly match any of the sampled scenarios anyway. Nevertheless, if the choice of surrogate PF model used in the recourse stage affects the optimal mitigation, then it raises the question if one or more of those models are not suitable for this application.

For the vast majority of the instances we studied, the optimal mitigation solutions were uniquely optimal. We determined this computationally by adding the no-good cut $(\mathbf{1} - \mathbf{x}^*)^\top \mathbf{x} \geq 1$ to the instance, solving that restricted instance to optimality, and assessing the objective value. In this cut, \mathbf{x}^* is the identified optimal solution, \mathbf{x} is the vector of decision variables, and $\mathbf{1}$ is the all-ones vector. For the vector of resource costs \mathbf{c} , if $\mathbf{c}^\top \mathbf{x}^* = f$, then the only solution cut from the feasible space is \mathbf{x}^* . Otherwise, this constraint cuts all $\mathbf{x} \geq \mathbf{x}^*$ (*i.e.*, all the solutions that implement \mathbf{x}^* and possibly more). Despite mitigating more flooding, such solutions are no better performing than \mathbf{x}^* which, recall, is optimal.

We attribute the frequent occurrence of unique optimal mitigation solutions to the power grid instance having little symmetry. The few instances with multiple mitigation optima typically have one or more resources that cannot be used effectively and are instead deployed arbitrarily. As an example, consider a deterministic instance in which only one bus, a load bus, is affected. If 2 resources are required to prevent flooding at the associated substation, but only 1 resource is available, then that resource may be deployed arbitrarily with no effect. For the few instances having multiple mitigation optima, we did not bother identifying all optima as the task is computationally burdensome. Nevertheless, because most instances have a unique mitigation optimum, the vast majority of our mitigation solution comparisons are not subject to the doubt that arises from not having identified all of the multiple optima.

4.4.1. Impact of Power Flow Model. To determine the impact of the choice of power flow model on the optimal mitigation decisions, we performed several pairwise comparisons of mitigation solutions prescribed under our various PF models. For the Imelda case study, we compared every pair of PF models for budgets from 1 to 20 in the SP model and from 1 to 9 in the RO model. For Harvey, we compared DC and LPAC-L for budgets from 1 to 193 in the SP model and from 1 to 62 in the RO model. This amounted to 429 comparisons. To assess the similarity of two mitigation solutions, we employed an absolute measure from our past work (Austgen et al. 2021) and an analogous relative measure:

$$\text{AbsSim}(\mathbf{x}_A, \mathbf{x}_B; \mathbf{c}) = \mathbf{x}_A^\top \text{diag}(\mathbf{c}) \mathbf{x}_B, \quad (32)$$

$$\text{RelSim}(\mathbf{x}_A, \mathbf{x}_B; \mathbf{c}) = \frac{\mathbf{x}_A^\top \text{diag}(\mathbf{c}) \mathbf{x}_B}{\max\{\mathbf{c}^\top \mathbf{x}_A, \mathbf{c}^\top \mathbf{x}_B\}}. \quad (33)$$

In these definitions, $\text{diag}(\cdot)$ denotes the matrix having the argument as its diagonal. The absolute measure, a weighted inner product, captures the number of resources deployed in the

Table 4 A summary of instances for which the solutions differed depending on the chosen power flow model.

Case Study	Model	Budget	Power Flow Models		AbsSim	RelSim	Opt. Gaps (%)	
Imelda	SP	4	DC	LPAC-T	2	0.5000	0.9730	1.1138
Imelda	SP	4	DC	QPAC	2	0.5000	0.1559	1.1138
Imelda	SP	4	LPAC-L	LPAC-T	2	0.5000	0.9730	1.1284
Imelda	SP	4	LPAC-L	QPAC	2	0.5000	0.1559	1.1284
Imelda	RO	2	DC	LPAC-T	1	0.5000	2.6918	3.6036
Imelda	RO	2	DC	QPAC	1	0.5000	0.2754	3.6036
Imelda	RO	2	LPAC-L	LPAC-T	1	0.5000	2.6918	3.5914
Imelda	RO	2	LPAC-L	QPAC	1	0.5000	0.2754	3.5914
Imelda	RO	2	LPAC-T	QPAC	1	0.5000	0.0011	0.0000
Harvey	SP	88	DC	LPAC-L	85	0.9659	0.1100	0.1082
Harvey	SP	110	DC	LPAC-L	107	0.9727	0.0175	0.0179
Harvey	SP	114	DC	LPAC-L	110	0.9649	0.0009	0.0008
Harvey	SP	117	DC	LPAC-L	113	0.9658	0.0009	0.0008
Harvey	SP	128	DC	LPAC-L	118	0.9219	0.0137	0.0049
Harvey	SP	130	DC	LPAC-L	127	0.9769	0.0006	0.0009
Harvey	SP	137	DC	LPAC-L	133	0.9708	0.0061	0.0026
Harvey	SP	140	DC	LPAC-L	137	0.9785	0.0064	0.0025
Harvey	SP	144	DC	LPAC-L	141	0.9792	0.0064	0.0025
Harvey	SP	148	DC	LPAC-L	141	0.9527	0.0031	0.0056
Harvey	SP	150	DC	LPAC-L	147	0.9800	0.0064	0.0024
Harvey	SP	156	DC	LPAC-L	153	0.9808	0.0005	0.0007
Harvey	SP	164	DC	LPAC-L	161	0.9817	0.0021	0.0044
Harvey	SP	177	DC	LPAC-L	174	0.9831	0.0020	0.0020
Harvey	SP	186	DC	LPAC-L	183	0.9839	0.0021	0.0200
Harvey	RO	1	DC	LPAC-L	1	0.0000	0.0087	0.0000
Harvey	RO	5	DC	LPAC-L	5	0.6000	0.0158	0.0005
Harvey	RO	34	DC	LPAC-L	34	0.9118	0.0003	0.0000
Harvey	RO	35	DC	LPAC-L	35	0.9143	0.0003	0.0000
Harvey	RO	36	DC	LPAC-L	36	0.8889	0.0110	0.0020

same manner. The relative measure normalizes the quantity to a proportion of the number of resources needed by the more resource-intensive solution. Among the 429 comparisons, there were only 29 cases in which the solutions differed. Those differences are listed in Table 4. In the table, the two columns with relative optimality gap values are for the solution induced by the former power flow model evaluated in the latter (left) and vice versa (right).

For solutions from instances with small resource budgets, the relative similarity tends to be smaller. This is expected, however, since a small absolute difference in resource allocation impacts the normalized similarity measure more when the solutions being compared use fewer resources. In contrast, the similarity of solutions from instances with large resource budgets tend to be much higher.

In cases where the mitigation solutions were similar but not the same, we hypothesized that similar mitigation solutions would perform similarly if fixed in a model regardless of which PF model were to be incorporated in the second stage. We tested this hypothesis

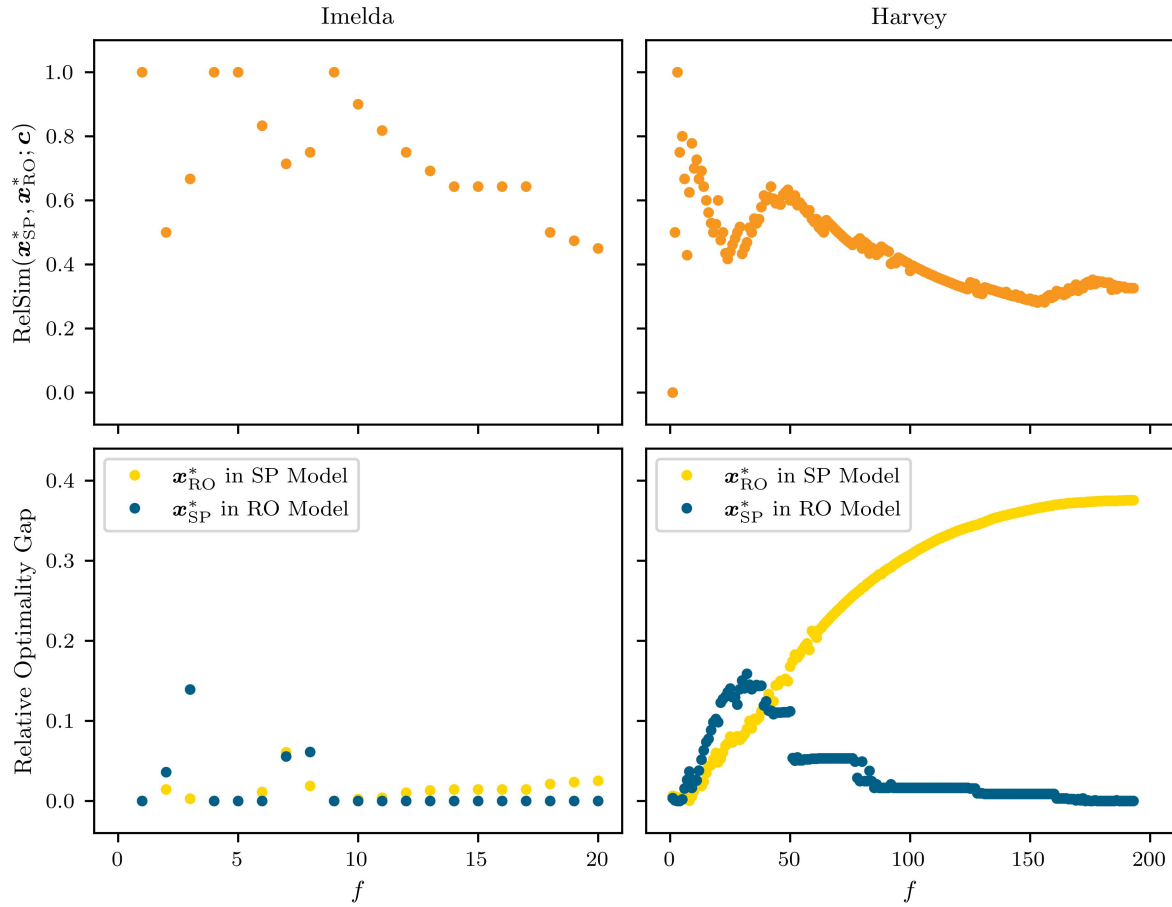


Figure 9 The optimal SP and RO solutions tend not to be very similar, especially for larger budgets.

for all 29 cases and found it to be true. In fact, we found differing solutions performed comparably even when they were not remarkably similar. For all pairs of differing mitigation solutions, we evaluated each solution in the model that prescribed the other and observed the optimality gaps to be quite small. The optimality gaps never exceeded 3.6% for Imelda instances and never exceeded 0.11% for Harvey instances. This analysis indicates the fidelity offered by more intricate PF models is minimally impactful on mitigation decision making, a key conclusion of this paper.

4.4.2. Impact of Uncertainty Perspective. In Section 3.4, we discussed the uncertainty perspectives associated with the SP and RO models. We investigated how differently the two models prescribe mitigation decisions by computing the similarity of optimal solutions subject to the same resource budget. For the models incorporating our adaptation of the DC approximation, these similarities are illustrated in Figure 9.

Because $\bar{f}_{\text{RO}} < \bar{f}_{\text{SP}}$ in both case studies, comparisons for $f > \bar{f}_{\text{RO}}$ involve the mitigation from the SP model with budget f and the mitigation from the RO model with fixed budget \bar{f}_{RO} . Consequently, the relative optimality gap of \mathbf{x}_{SP}^* in the RO model generally improves, and the relative optimality gap for \mathbf{x}_{RO}^* in the SP model monotonically worsens as f increases for $f > \bar{f}_{\text{RO}}$. In both case studies, the optimal solutions of the two models often differ considerably. In the Imelda case study, we observed that \mathbf{x}_{RO}^* performs well in the SP model and likewise for \mathbf{x}_{SP}^* in the RO model. This is likely a consequence of the Imelda flooding scenarios being so similar, as this phenomenon is not observed in the Harvey case study which has greater variance in the flooding scenarios.

Qualitatively, \mathbf{x}_{SP}^* is characterized by a relatively widespread allocation of the mitigation resources across the substations whereas \mathbf{x}_{RO}^* tends to exhibit more concentrated allocation. In Figure 10, this is illustrated for the case of $f = \bar{f}_{\text{RO}} = 62$ in the Harvey case study. On the left, we see \mathbf{x}_{SP}^* sites level $r = 1$ mitigation at 19 substations (yellow) and level $r = 2$ at 10 (orange); on the right, however, \mathbf{x}_{RO}^* sites level $r = 1$ mitigation at only 10 substations and level $r = 2$ at 14. Intuitively, the former solution is fit to minimize the expected loss over all flooding scenarios and thus must cover more assets. In contrast, the latter solution is fit to address only the scenarios that induce the worst outcomes.

5. Conclusions

In this paper, we proposed using two-stage optimization modeling to inform power grid flood mitigation decision making prior to an imminent and uncertain hurricane, and we formulated the problem as both a stochastic programming model and a robust optimization model. To capture the consequences of flooding on the power grid, we introduced novel adaptations of the DC and LPAC power flow approximations with relatively complete recourse and use these models as the second-stage recourse problems. We applied these models to a pair of case studies featuring the ACTIVS 2000-bus synthetic grid of Texas and geographically realistic flooding scenarios derived from historical Tropical Storm Imelda and Hurricane Harvey data.

In a comprehensive computational study, we analyzed the impact of the choice of PF model, the mitigation budget, and the uncertainty perspective on the optimal mitigation decisions. For fixed mitigation budget and uncertainty perspective, we observed the choice of PF model has little to no bearing on the optimal mitigation decisions and objective values but has a remarkable impact on the time required to solve the model to optimality. Because

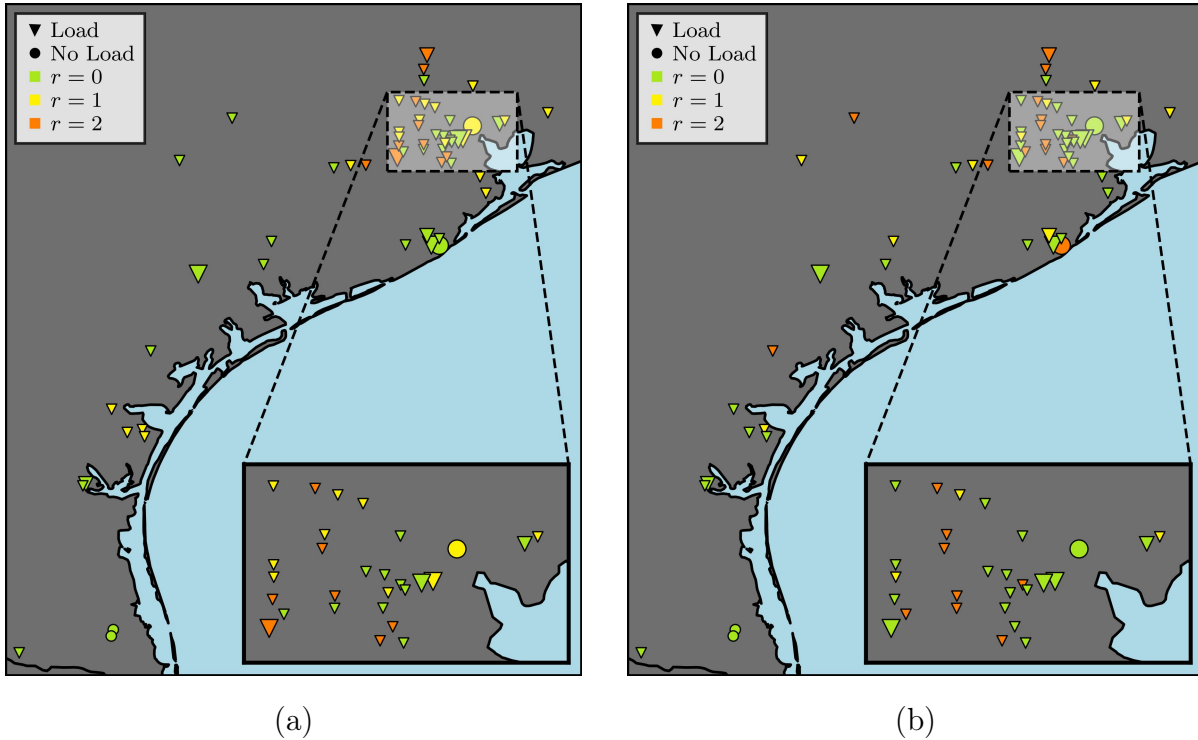


Figure 10 In (a), the SP solution is characterized by a relatively widespread allocation of resources whereas in (b) the RO solution exhibits a more concentrated allocation of resources.

the model is solved most quickly when our adapted DC model is used, it should be preferred to our adapted LPAC-L, LPAT-T, and QPAC models for this application despite its lower fidelity.

For fixed mitigation budget and PF model, we found the adopted uncertainty perspective (*i.e.*, stochastic programming model vs robust optimization model) has a significant impact on the optimal mitigation decisions. However, the decision maker’s belief that either “nature is fair” or “nature is adversarial” is a matter of personal preference. Ergo, we only recommend a potential decision maker weigh the merits of these two belief systems well in advance of committing to one for flood planning.

For fixed PF model and uncertainty perspective, we generally observed decreasing returns as the mitigation budget increases. This suggests that, depending on the relative cost of mitigation and load shed, it might not be cost-beneficial to mitigate all preventable flooding. Our model could be adapted to determining the optimal number of Tiger DamsTM to stockpile. However, that is a mid- to long-term decision problem that necessitates evaluation over a larger and broader set of flooding scenarios. The models we formulated in this paper are best suited for quickly prescribing mitigation using a predetermined quantity of Tiger DamsTM prior to an imminent flooding event.

Ultimately, our results indicate our models and methods are capable of prescribing strategies for reducing initial hurricane impacts by over 43% compared to the base “do nothing” solution using Tiger Dam™ flood barriers up to one meter tall. Such improvements highlight the potential for Tiger Dam™ barriers to prevent power grid damages and for our models to prescribe their effective deployment.

In the future, we expect to improve the model in two ways. First, we would like to extend the recourse problem to include multiple time periods. Presently, we rely on performance under a single representative demand profile. Using a multi-time period model would allow us to more accurately capture temporal variability like the daily periodicity of demand and renewable generation and temporal constraints like generator ramp rate limits. We believe this would improve the applicability of the prescribed solutions to reality. Of course, this would increase the complexity of the recourse problem and assuredly require more time to solve the model. Should it prove to be too difficult a model to solve, we could at the very least attempt to validate the prescribed solutions in multi-time period scenarios. Second, resilience in this paper was quantified by expected system-wide load shed, but other objectives or side constraints related to performance may be considered. Alternatives such as the joint minimization of mitigation and load shed costs, equity-related metrics, service level constraints, chance constraints, etc. may be considered in the future.

Acknowledgments

We the authors thank The University of Texas Energy Institute for funding our “Defending the Electricity Infrastructure Against Extreme Weather Events, Now & in the Future” research project as part of the “Fueling a Sustainable Energy Transition” initiative.

We also acknowledge the Texas Advanced Computing Center (TACC) at The University of Texas at Austin for providing HPC and data visualization resources that have contributed to the research results reported within this paper. URL: <http://www.tacc.utexas.edu>

Finally, we are grateful for several individual contributions to this work by current and former members of our research team at The University of Texas at Austin. Namely, we thank Dr. Zong-Liang Yang, Dr. Carey King, Dr. Wen-Ying Wu, Dr. Kyoung Yoon Kim, Joshua Yip, and Ashutosh Shukla.

References

- Arab A, Khodaei A, Khator SK, Ding K, Emesih VA, Han Z (2015) Stochastic pre-hurricane restoration planning for electric power systems infrastructure. *IEEE Transactions on Smart Grid* 6(2):1046–1054, URL <http://dx.doi.org/10.1109/TSG.2015.2388736>.

- Asghari M, Fathollahi-Fard AM, Mirzapour Al-e hashem SMJ, Dulebenets MA (2022) Transformation and linearization techniques in optimization: A state-of-the-art survey. *Mathematics* 10(2), ISSN 2227-7390, URL <http://dx.doi.org/10.3390/math10020283>.
- Austgen B, Gupta S, Kutanoglu E, Hasenbein J (2022) Stochastic hurricane flood mitigation for power grid resilience. *2022 IEEE Power & Energy Society General Meeting (PESGM)*, 1–5, URL <http://dx.doi.org/10.1109/PESGM48719.2022.9916992>.
- Austgen B, Hasenbein J, Kutanoglu E (2021) Impacts of approximate power flow models on optimal flood mitigation in a stochastic program. *IIE Annual Conference Proceedings*, 518–523.
- Austgen B, Kutanoglu E, Hasenbein JJ (2023) A two-stage stochastic programming model for electric substation flood mitigation prior to an imminent hurricane, URL <http://dx.doi.org/10.48550/ARXIV.2302.10996>, submitted.
- Baker K (2021) Solutions of DC OPF are never AC feasible. *Proceedings of the Twelfth ACM International Conference on Future Energy Systems*, 264–268, e-Energy '21 (New York, NY, USA: Association for Computing Machinery), ISBN 978-1-4503-8333-2, URL <http://dx.doi.org/10.1145/3447555.3464875>.
- Ben-Tal A, Ghaoui L, Nemirovski A (2009) *Robust Optimization*. Princeton Series in Applied Mathematics (Princeton University Press), ISBN 978-1-4008-3105-0.
- Birchfield AB, Xu T, Gegner KM, Shetye KS, Overbye TJ (2017) Grid structural characteristics as validation criteria for synthetic networks. *IEEE Transactions on Power Systems* 32(4):3258–3265, URL <http://dx.doi.org/10.1109/TPWRS.2016.2616385>.
- Birge JR, Louveaux F (2011) *Introduction to Stochastic Programming* (Springer Science & Business Media).
- Blake ES, Zelinsky DA (2018) Hurricane Harvey. Technical Report AL092017, National Hurricane Center, URL https://www.nhc.noaa.gov/data/tcr/AL092017_Harvey.pdf.
- Byrd RH, Nocedal J, Waltz RA (2006) Knitro: An integrated package for nonlinear optimization. Di Pillo G, Roma M, eds., *Large-Scale Nonlinear Optimization*, 35–59 (Boston, MA: Springer US), ISBN 978-0-387-30065-8, URL http://dx.doi.org/10.1007/0-387-30065-1_4.
- Coffrin C, Hentenryck PV, Bent R (2011) Strategic stockpiling of power system supplies for disaster recovery. *2011 IEEE Power and Energy Society General Meeting*, 1–8.
- Coffrin C, Hijazi H, Van Hentenryck P (2020) Alternating current (AC) power flow analysis in an electrical power network. US Patent 10,591,520.
- Coffrin C, Van Hentenryck P (2014) A linear-programming approximation of AC power flows. *INFORMS Journal on Computing* 26(4):718–734, URL <http://dx.doi.org/10.1287/ijoc.2014.0594>.
- Coffrin C, Van Hentenryck P (2015) Transmission system restoration with co-optimization of repairs, load pickups, and generation dispatch. *International Journal of Electrical Power & Energy Systems* 72:144–154, ISSN 01420615, URL <http://dx.doi.org/10.1016/j.ijepes.2015.02.027>.

- Czyzyk J, Mesnier MP, Moré JJ (1998) The NEOS server. *IEEE Journal on Computational Science and Engineering* 5(3):68–75.
- Dolan ED (2001) The NEOS server 4.0 administrative guide. Technical Memorandum ANL/MCS-TM-250, Mathematics and Computer Science Division, Argonne National Laboratory.
- Dvorkin Y, Henneaux P, Kirschen DS, Pandžić H (2018) Optimizing primary response in preventive security-constrained optimal power flow. *IEEE Systems Journal* 12(1):414–423, ISSN 1937-9234, URL <http://dx.doi.org/10.1109/JSYST.2016.2527726>, conference Name: IEEE Systems Journal.
- Elizondo MA, Fan X, Davis SH, Vyakaranam BG, Ke X, Barrett EL, Newman SF, Royer PD, Etingov PV, Tbaileh A, Wang H, Agrawal U, Du W, Weidert PJ, Lewis DA, Franklin TP, Samaan NA, Makarov YV, Dagle JE (2020) Risk-based dynamic contingency analysis applied to Puerto Rico electric infrastructure. Technical report, Pacific Northwest National Lab (PNNL), URL <http://dx.doi.org/10.2172/1771798>.
- Garcia M, Austgen B, Pierre B, Hasenbein J, Kutanoglu E (2022) Risk-averse investment optimization for power system resilience to winter storms. *2022 IEEE/PES Transmission and Distribution Conference and Exposition (T D)*.
- Garifi K, Johnson ES, Arguello B, Pierre BJ (2022) Transmission grid resiliency investment optimization model with SOCP recovery planning. *IEEE Transactions on Power Systems* 37(1):26–37, URL <http://dx.doi.org/10.1109/TPWRS.2021.3091538>.
- Gropp W, Moré JJ (1997) Optimization environments and the NEOS server. Buhman MD, Iserles A, eds., *Approximation Theory and Optimization*, 167 – 182 (Cambridge University Press).
- Gurobi Optimization, LLC (2022) Gurobi Optimizer Reference Manual. URL <https://www.gurobi.com>.
- Huang L, Lai CS, Zhao Z, Yang G, Zhong B, Lai LL (2022) Robust N-k security-constrained optimal power flow incorporating preventive and corrective generation dispatch to improve power system reliability. *CSEE Journal of Power and Energy Systems* 1–14, ISSN 2096-0042, URL <http://dx.doi.org/10.17775/CSEEJPES.2021.06560>, conference Name: CSEE Journal of Power and Energy Systems.
- IEEE2022 (2022) IEEE guide for electric power distribution reliability indices. *IEEE Std 1366-2022 (Revision of IEEE Std 1366-2012)* 1–44, URL <http://dx.doi.org/10.1109/IEEESTD.2022.9955492>, Conference Name: IEEE Std 1366-2022 (Revision of IEEE Std 1366-2012).
- ISER2023 (2022) ISER - Electric Disturbance Events (DOE-417). URL <https://www.oe.net1.doe.gov/oe417.aspx>.
- Kile H, Uhlen K, Warland L, Kjølle G (2014) A comparison of AC and DC power flow models for contingency and reliability analysis. *2014 Power Systems Computation Conference*, 1–7, URL <http://dx.doi.org/10.1109/PSCC.2014.7038459>.
- Knutson T, Camargo SJ, Chan JCL, Emanuel K, Ho CH, Kossin J, Mohapatra M, Satoh M, Sugi M, Walsh K, Wu L (2020) Tropical cyclones and climate change assessment: Part II: Projected response

- to anthropogenic warming. *Bulletin of the American Meteorological Society* 101(3):E303 – E322, URL <http://dx.doi.org/10.1175/BAMS-D-18-0194.1>, place: Boston MA, USA Publisher: American Meteorological Society.
- Latto A, Berg R (2020) Tropical Storm Imelda. Technical Report AL112019, National Hurricane Center, URL https://www.nhc.noaa.gov/data/tcr/AL112019_Imelda.pdf.
- Linkov I, Trump BD (2019) *The Science and Practice of Resilience* (Springer), URL <https://link.springer.com/book/10.1007/978-3-030-04565-4>.
- Liu H, Tesfatsion L, Chowdhury AA (2009) Locational marginal pricing basics for restructured wholesale power markets. *2009 IEEE Power & Energy Society General Meeting*, 1–8, URL <http://dx.doi.org/10.1109/PES.2009.5275503>.
- Logan TM, Aven T, Guikema SD, Flage R (2022) Risk science offers an integrated approach to resilience. *Nature Sustainability* 5(9):741–748, ISSN 2398-9629, URL <http://dx.doi.org/10.1038/s41893-022-00893-w>, number: 9 Publisher: Nature Publishing Group.
- Mohagheghi S, Rebennack S (2015) Optimal resilient power grid operation during the course of a progressing wildfire. *International Journal of Electrical Power & Energy Systems* 73:843–852, ISSN 0142-0615, URL <http://dx.doi.org/10.1016/j.ijepes.2015.05.035>.
- Molzahn DK, Hiskens IA (2019) A Survey of Relaxations and Approximations of the Power Flow Equations. *Foundations and Trends® in Electric Energy Systems* 4(1-2):1–221, ISSN 2332-6557, URL <http://dx.doi.org/10.1561/31000000012>.
- Monticelli A, Pereira M, Granville S (1987) Security-constrained optimal power flow with post-contingency corrective rescheduling. *IEEE Transactions on Power Systems* 2(1):175–180, publisher: IEEE.
- Moreno R, Panteli M, Mancarella P, Rudnick H, Lagos T, Navarro A, Ordonez F, Araneda JC (2020) From reliability to resilience: Planning the grid against the extremes. *IEEE Power and Energy Magazine* 18(4):41–53, ISSN 1558-4216, URL <http://dx.doi.org/10.1109/MPE.2020.2985439>, conference Name: IEEE Power and Energy Magazine.
- Movahednia M, Kargarian A (2022) Flood-aware Optimal Power Flow for Proactive Day-ahead Transmission Substation Hardening. *2022 IEEE Texas Power and Energy Conference (TPEC)*, 1–5, URL <http://dx.doi.org/10.1109/TPEC54980.2022.9750830>.
- NCEI2022 (2022) U.S. billion-dollar weather and climate disasters. Technical report, NOAA National Centers for Environmental Information (NCEI), URL <http://dx.doi.org/10.25921/stkw-7w73>.
- NERC2022 (2022) Reliability Standards for the Bulk Electric Systems of North America.
- NRC2012 (2012) *Disaster resilience: A national imperative*. ISBN 978-0-309-26150-0, URL <http://dx.doi.org/10.17226/13457>.
- Overbye T, Cheng X, Sun Y (2004) A comparison of the AC and DC power flow models for LMP calculations. *37th Annual Hawaii International Conference on System Sciences, 2004. Proceedings of the*, URL <http://dx.doi.org/10.1109/HICSS.2004.1265164>.

- Paul B, Pathak MK, Pal J, Chanda CK (2017) A comparison of locational marginal prices and locational load shedding marginal prices in a deregulated competitive power market. *2017 IEEE Calcutta Conference (CALCON)*, 46–50, URL <http://dx.doi.org/10.1109/CALCON.2017.8280693>.
- Pierre BJ, Arguello B, Staid A, Guttromson RT (2018) Investment optimization to improve power system resilience. *2018 IEEE International Conference on Probabilistic Methods Applied to Power Systems (PMAPS)*, 1–6, URL <http://dx.doi.org/10.1109/PMAPS.2018.8440467>.
- Quarm E, Fan X, Elizondo M, Madani R (2022) Proactive posturing of large power grid for mitigating hurricane impacts. *2022 IEEE Power & Energy Society Innovative Smart Grid Technologies Conference (ISGT)*, 1–5, URL <http://dx.doi.org/10.1109/ISGT50606.2022.9817529>.
- Sahraei-Ardakani M, Ou G (2017) Day-ahead preventive scheduling of power systems during natural hazards via stochastic optimization. *2017 IEEE Power Energy Society General Meeting*, 1–1, URL <http://dx.doi.org/10.1109/PESGM.2017.8274453>.
- Shukla A, Austgen B, Kutanoglu E, Hasenbein J (2022) Budget allocation in optimizing power grid resilience to extreme weather: Hardening, preparation, or recovery? *IIE Annual Conference Proceedings*, 1–6.
- Shukla A, Hasenbein J, Kutanoglu E (2021) A scenario-based optimization approach for electric grid substation hardening against storm surge flooding. *IIE Annual Conference Proceedings*, 1004–1009.
- Souto L, Yip J, Wu WY, Austgen B, Kutanoglu E, Hasenbein J, Yang ZL, King CW, Santoso S (2022) Power system resilience to floods: Modeling, impact assessment, and mid-term mitigation strategies. *International Journal of Electrical Power & Energy Systems* 135:107545, ISSN 0142-0615, URL <http://dx.doi.org/https://doi.org/10.1016/j.ijepes.2021.107545>.
- Tan Y, Das AK, Arabshahi P, Kirschen DS (2018) Distribution systems hardening against natural disasters. *IEEE Transactions on Power Systems* 33(6):6849–6860, URL <http://dx.doi.org/10.1109/TPWRS.2018.2836391>.
- Watson JP, Guttromson R, Silva-Monroy C, Jeffers R, Jones K, Ellison J, Rath C, Gearhart J, Jones D, Corbet T, Hanley C, Walker LT (2014) Conceptual framework for developing resilience metrics for the electricity, oil, and gas sectors in the United States. Technical report, Sandia National Laboratories, URL <http://dx.doi.org/10.2172/1177743>.
- Webster PJ, Holland GJ, Curry JA, Chang HR (2005) Changes in tropical cyclone number, duration, and intensity in a warming environment. *Science* 309(5742):1844–1846, URL <http://dx.doi.org/10.1126/science.1116448>.
- Zhang H, Vittal V, Heydt GT, Quintero J (2012) A mixed-integer linear programming approach for multi-stage security-constrained transmission expansion planning. *IEEE Transactions on Power Systems* 27(2):1125–1133, ISSN 1558-0679, URL <http://dx.doi.org/10.1109/TPWRS.2011.2178000>, conference Name: IEEE Transactions on Power Systems.